Submitted to the Journal of Geophysical Research

LBL-10617 c.2
Preprint

A PLAUSIBLE TWO-DIMENSIONAL VERTICAL MODEL OF THE EAST MESA GEOTHERMAL FIELD, CALIFORNIA, U.S.A.

K. P. Goyal and D. R. Kassoy

March 1980

Prepared for the U.S. Department of Energy
under Contract W-7405-ENG-48

DISCLAIMER

A PLAUSIBLE TWO-DIMENSIONAL VERTICAL MODEL OF THE EAST MESA GEOTHERMAL FIELD, CALIFORNIA, U.S.A.

K. P. Goyal
Earth Sciences Division
Lawrence Berkeley Laboratory
University of California
Berkeley, California 94720

and

D. R. Kassoy
Mechanical Engineering Department,
University of Colorado,
Boulder, Colorado, 80309.

A two-dimensional conceptual model of the East Mesa geothermal system is developed on the basis of the existing geological, geophysical geochemical, heat flux, and borehole logging data. A fault called the Mesa Fault is assumed to charge the reservoir, which is overlaid by a clay-rich cap. The mathematical model is based on the flow of liquid water in a saturated porous medium. To obtain temperature-depth distributions similar to those measured at the site, we assume that the liquid is convecting at a high Rayleigh number. In this approximation, liquid rises up the fault and spreads into the near regions of the reservoir isothermally. The cooling effect of the surface on the flow in the reservoir is confined to a thin layer adjacent to the cap-reservoir interface near the fault. This layer grows with the distance from the fault. Eventually, the full depth of the reservoir is cooled by the surface. Results are obtained for the velocities, pressures, and temperatures of the entire system (fault zone, aquifer and clay cap). Finally we compare the heat flux predicted for the surface to that measured at the site in shallow wells.

INTRODUCTION

Liquid-dominated geothermal anomalies exist in the Imperial Valley of southern California at the Salton Sea, Brawley, East Mesa, Dunes, and Heber areas as shown in Figure 1. The East Mesa anomaly has been considered for development of its geothermal resources by the Bureau of Reclamation, Magma Power Company, and Republic Geothermal Inc., and this interest has produced a significant body of field data for this anomaly. The geological, geophysical, geochemical and borehole logging data is described in Black [1975], Bailey [1977] and several U.S. Bureau of Reclamation reports [1972, 1973, 1974, 1977]. A case history of the field is given by Davis and Sanyal [1979], and a thorough survey is contained in the work of Howard et al. [1978].

A conceptual model of the East Mesa anomaly was developed by Bailey [1977], based on the available field data. Goyal [1978] described a mathematical model for the system, based on saturated flow in porous media. A simplified version has been described in Goyal and Kassoy [1980]. Riney et al. [1979a] have described a closely related model.

In the present paper, we describe a two-dimensional vertical model of the East Mesa system that includes an impermeable clay cap ingnored in Goyal and Kassoy [1980]. Our preliminary goal is to show that the concept of fault-zone-controlled charging of a geothermal reservoir like that at East Mesa is plausible. To this end, we show that the shut-in well-bore temperature distributions with depth and near-surface heat flux patterns can be predicted with approximate quantitative accuracy. Of course, our simplified model, lacking many of the detailed features believed to exist at East Mesa, should not be thought of as the definitive description.

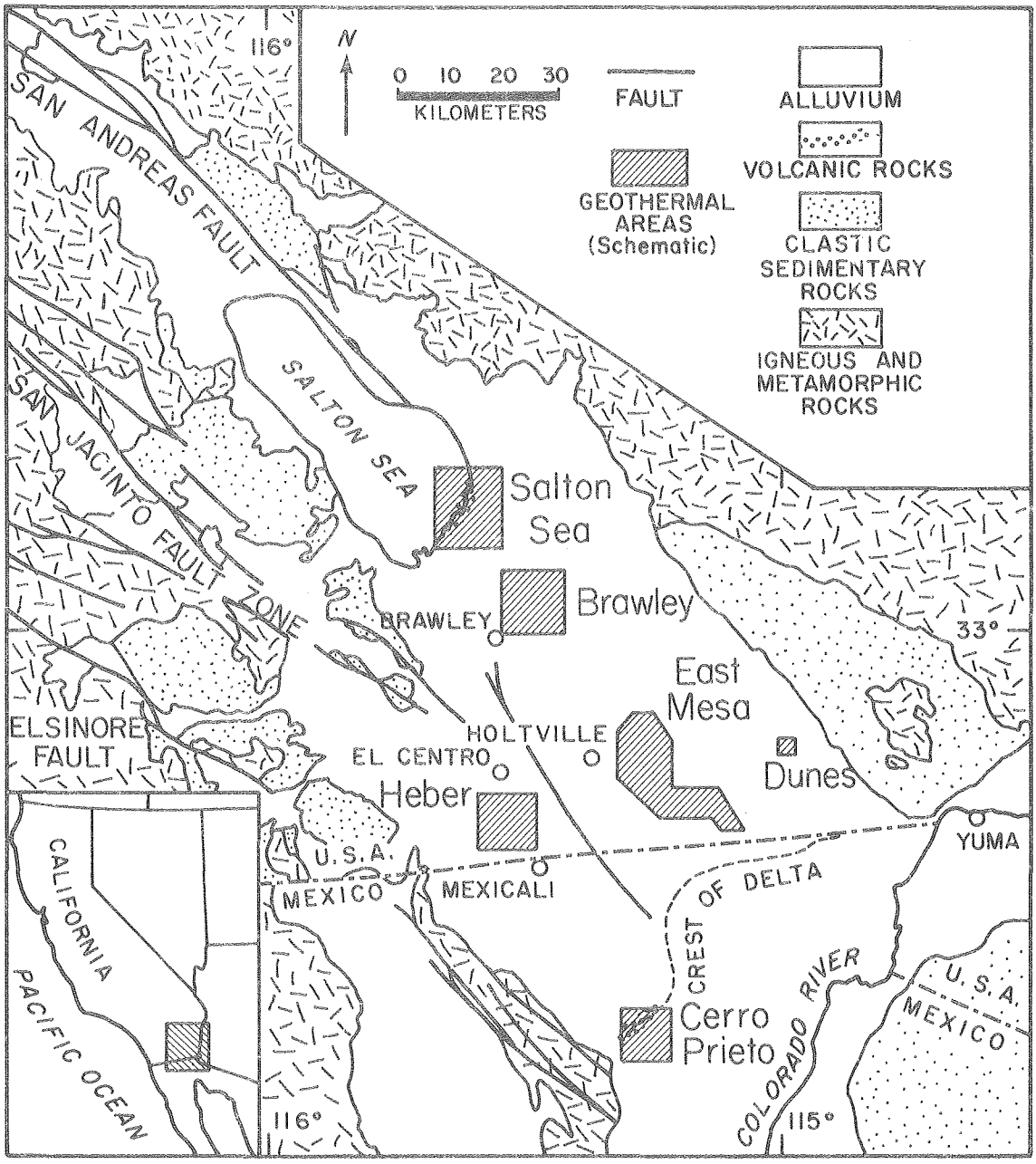

XBL 7912-13479

Figure 1. Geologic Map of the Imperial Valley, California, U.S.A. (Adapted from Elders et al. [1978].)

EAST MESA FIELD DATA

The East Mesa geothermal anomaly is located on the northern flank of the Colorado River delta and on the east side of a deep sediment-filled structural basin called the Salton Trough. The basin contains three main rock groups. A lower sequence of mainly nonmarine sedimentary rocks of early to middle Tertiary age dominate the basal unit which unconformably overlies pre-Tertiary metamorphic and igneous rocks. The marine Imperial formation of Pliocene age comprises the beds of the middle sequence. The upper sequence consists predominantly of nonmarine deposits of late Tertiary and Quaternary age derived mainly from the Colorado River drainage area. This upper sequence accounts for most of the valley fill in the central part of the trough. Within its thick accumulations of the young valley fill, the sediments of the Imperial Valley comprise a vast water reservoir. The horizontal permeability of the sediments is much larger than the vertical permeability because of the presence of platey and ellipsoidal grains often aligned during sedimentation. The existence of the lenticular clays also reduces the vertical permeability.

The structure of the Imperial Valley is controlled by numerous strike-slip faults of the San Andreas and San Jacinto fault system. Three faults with no surface expressions [Rex, 1970; Babcock, 1971; and Combs and Hadley, 1973] have been inferred at the Mesa anomaly by indirect means such as resistivity surveys, oblique aerial infrared photography and microseismic activity (Figure 2). The Combs-Hadley fault is also called the Mesa fault [Combs and Hadley, 1977]. Howard et al. [1978] inferred two nearly parallel faults based on the seismic and well log data. The position of one of these faults is very close to that of the Mesa fault (Figure 3).

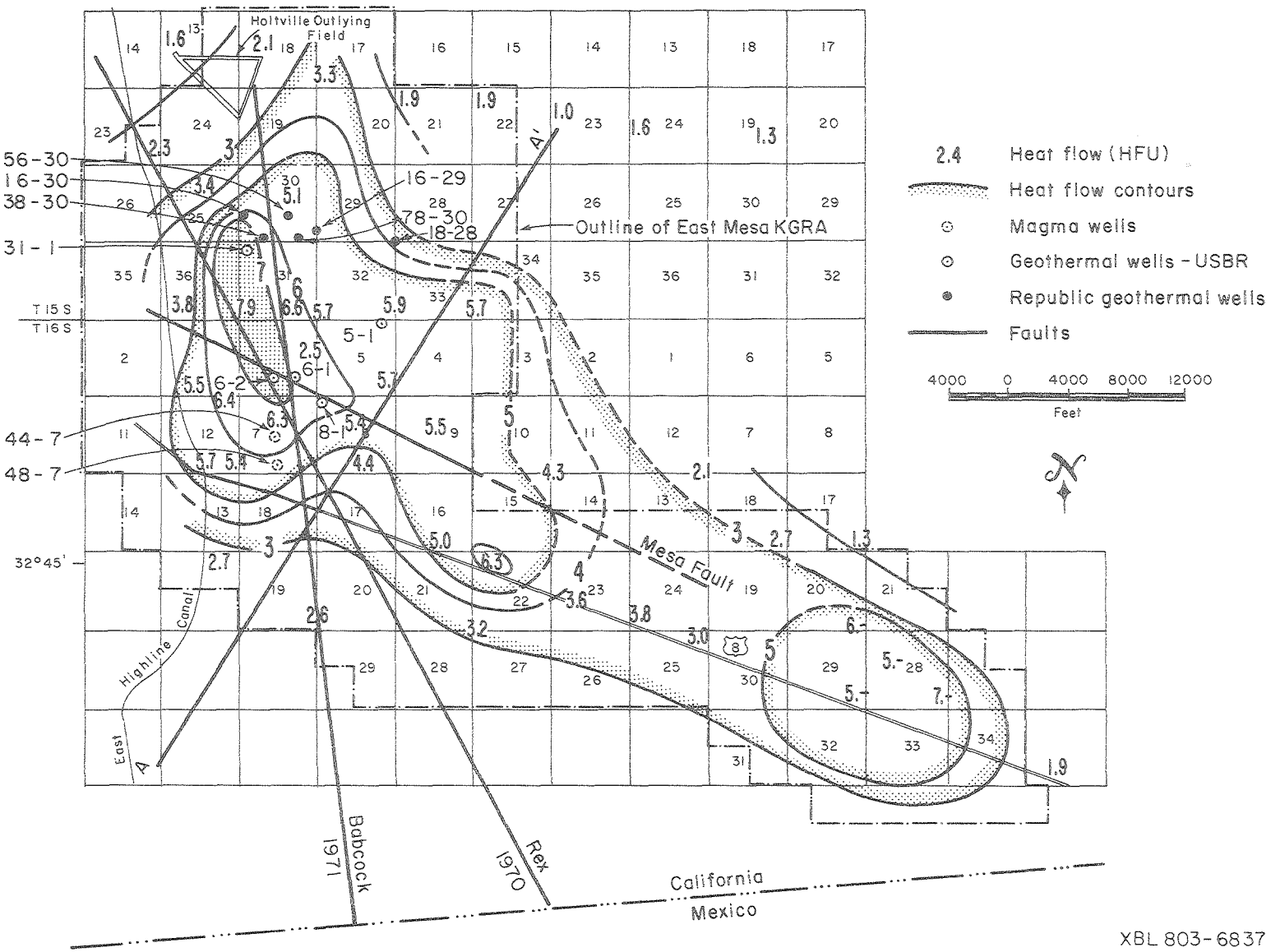

Figure 2. East Mesa KGRA (Known Geothermal Resource Areas) heat flow. (Adapted from U.S. Bureau of Reclamation Report, [1974].)

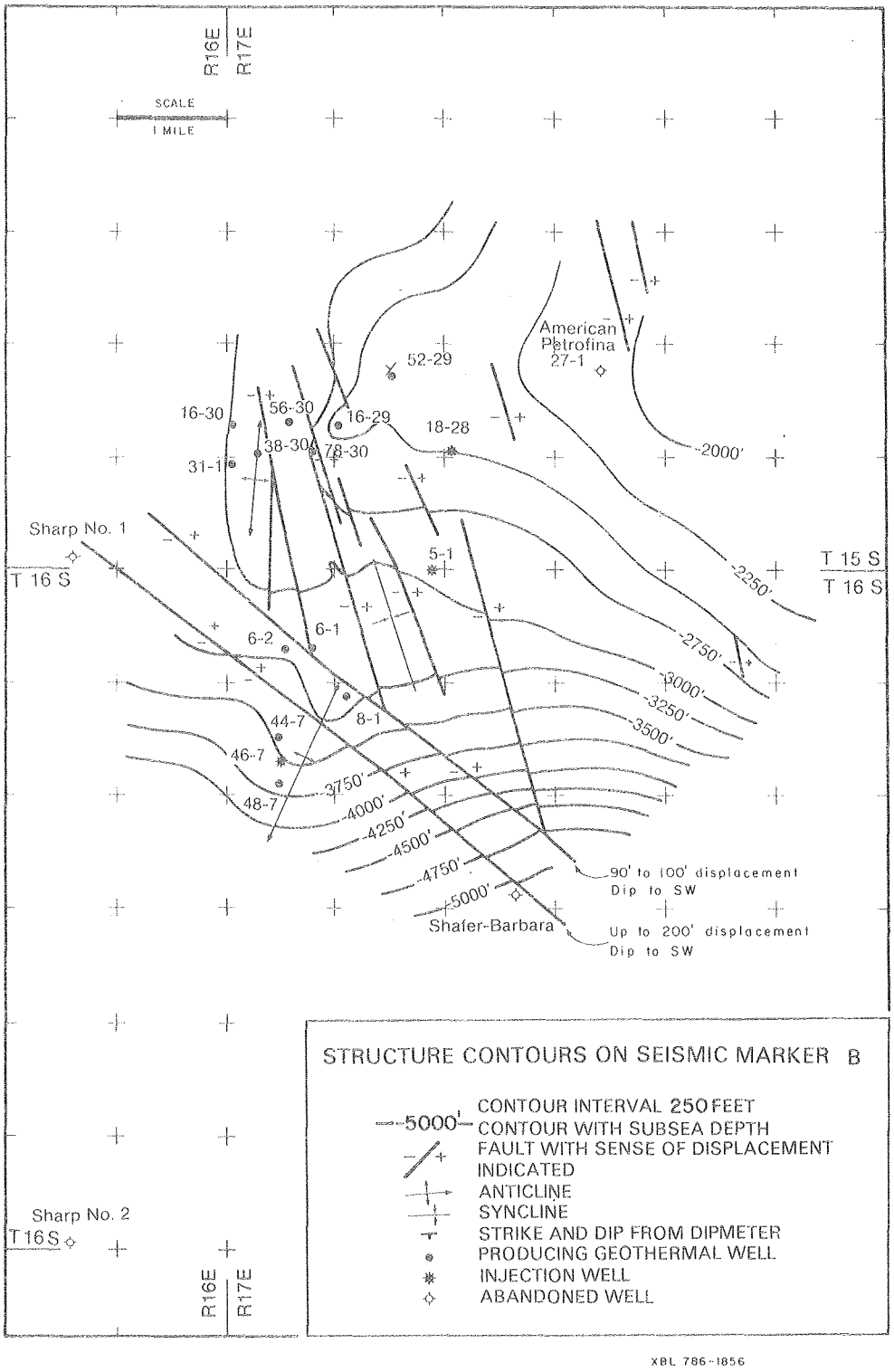

Figure 3. Location of faults on the basis of seismic and well log data. (Adapted from Howard et al. [1978].)

Electrical resistivity decreases with increasing temperature and increasing water salinity. Therefore, the combined effect of high salinity waters and high temperatures in a geothermal reservoir make electrical resistivity surveys a valuable tool in locating geothermal anomalies. Meidav and Furgerson [1971] made a detailed electrical resistivity study of the Imperial Valley at 305, 610 and 915 meters depth. Their results show a regional resistivity gradient which decreases northwestward from the southeast corner of the Imperial valley, near the Colorado River, to values about two orders of magnitude lower at the Salton Sea. Based on the resistivity surveys, the following conclusions can be derived: groundwater salinity increases with increasing distance from the Colorado River. Many of the faults in the Imperial Valley act as aquitards and restrict horizontal water movement. Resistivity lows are found at the East Mesa, Salton Sea, Heber, Brawley and Dunes geothermal anomalies.

Gravity studies of Biehler [1971] revealed the presence of a broad positive gravity anomaly throughout the Imperial Valley. It may be due to either an emplacement of high density crustal material beneath the trough axis or a thinner than average crust beneath the Imperial Valley. An increase in the density of the crustal material can be caused by clay diagenesis, cementation and/or thermal metamorphism. Some or all the above factors might be contributing to the gravity anomaly in the East Mesa area.

Combs and Hadley [1977] recorded microearthquakes associated with the East Mesa anomaly for five weeks during the summer of 1973 and defined a new right lateral strike-slip fault, called Mesa fault (Figure 2). The focal depths of the microearthquakes ranged from near surface to about 8 km. More than half of the located events have hypocenters

greater than 4 km which is approximately the depth to crystalline basement. This data shows that the fault is active both above and below the basement. A more recent microseismic study continuously conducted at East Mesa during the last 186 days of 1977 is described in Howard et al. [1978]. This latest study detected no local events within the East Mesa field for those six months, although a significant number of events with hypocenters located elsewhere in the Imperial Valley were recorded by the six-station instrument array positioned at East Mesa.

Areas of high near-surface heat flow are generally associated with active volcanism of geothermal areas [Bailey, 1977]. Figure 2 shows the heat flow contours and the locations of the test wells drilled in the East Mesa area by Republic Geothermal Inc., United States Bureau of Reclamation (USBR) and Magma Power Company. Republic Geothermal Inc. has drilled six wells to date, ranging in depth from 2.25 km to 2.77 km. Towards the south, the geothermal anomaly has been explored and assessed by USBR (five wells) and Magma Power Company (three wells). The position of the heat flow contours around Mesa fault confirms the hypothesis of Combs and Hadley [1977] that the Mesa fault acts as a conduit for rising geothermal fluids of the Mesa anomaly. Morrison et al. [1979] discovered a dipolar self-potential anomaly in the East Mesa field. Such anomalies are often associated with faults which are thought to serve as conduits for geothermal fluids, or with areas of high heat flow or vigorous subsurface fluid flow [Corwin et al., 1978]. The locations of the charging planes based on the self-potential study are shown in Figure 4. It can be noted in this figure that the charging plane A is located very near to Mesa fault and thus confirms the previously mentioned hypothesis.

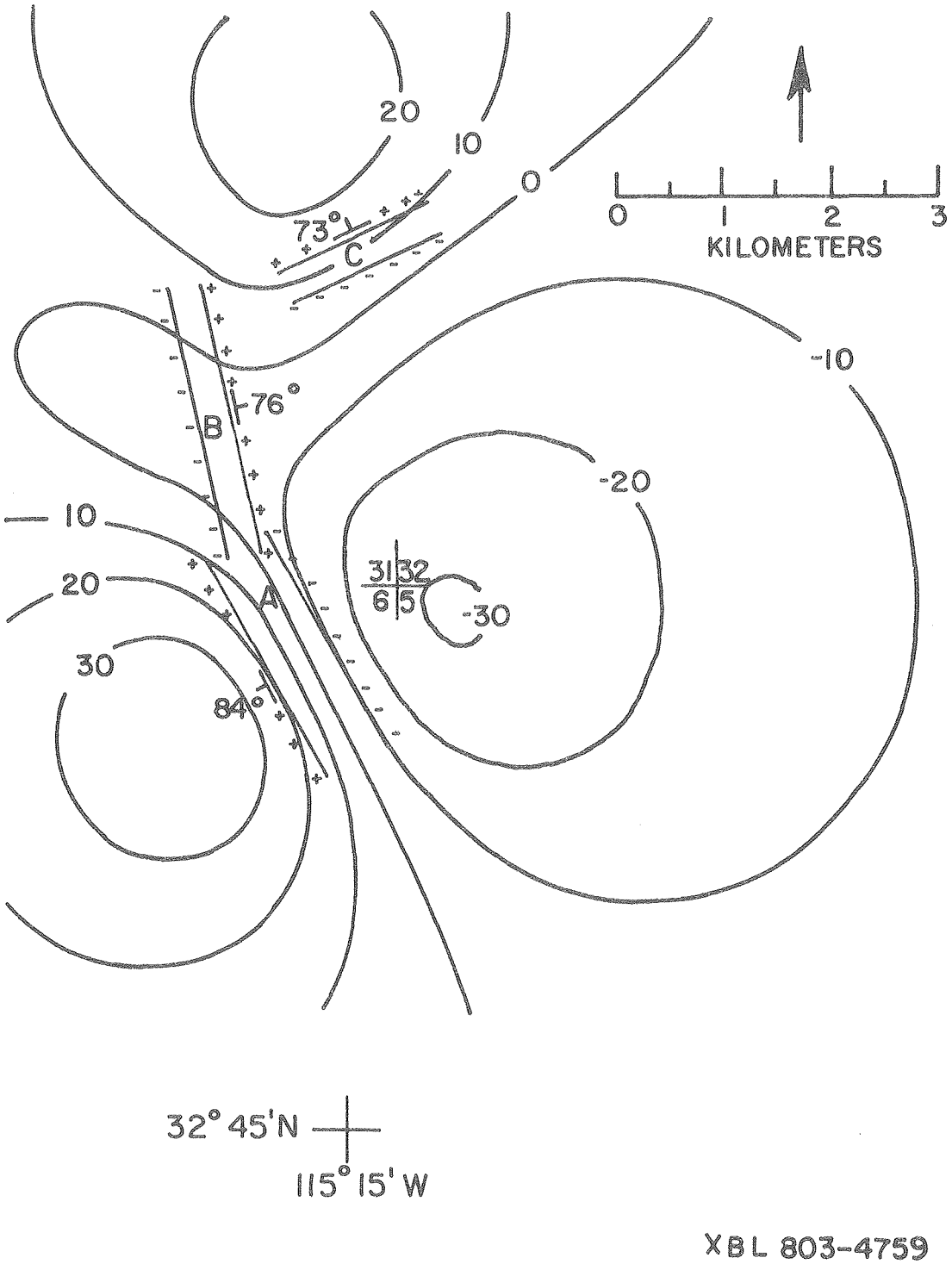

Figure 4. Self potential contours and inferred charging planes. (Adapted from Morrison et al. [1979].)

These charging planes range from about 300 to 600 m in width.

Borehole logging data indicate that the stratum in the upper 600 to 700 m is clay-dominated, below 2.1 km it is shale-dominated, and in the middle it is dominated by sands and sandstones. It is this part of the field that is considered to be a highly permeable zone consituting the geothermal reservoir. A plot of temperature versus depth in the wells shows three different gradients [Goyal, 1978]. Steep gradients in the upper 700-900 m are associated with vertical heat transfer by conduction. Presumably, the presence of large amounts of interbedded clays prevents vertical convection from occurring. Temperatures are less variable in the middle zone, which extends up to 1900-2100 m. Heat transfer in this zone is profoundly influenced by convection, which is possible in sandy zones of relatively high permeability. Steeper temperature gradients are seen below 1900-2100 m in Mesa Well 6-1. It would appear that the change in mode of heat transfer from convection to conduction at this depth is due to the presence of increasingly large amounts of shales in this zone. Figure 5 shows the temperature variations of the wells in the permeable zone of the anomaly. It can be seen that wells 6-1, 6-2, 8-1, 44-7, and 48-7 are the hottest in this area. Flat temperature profiles can be seen in wells 8-1, 48-7, and 44-7 between the depths 1200-1800 m, 1600-2100 m, and 1500-1850 m respectively. One could interpret these flat portions as zones that are strongly affected by fault zone flow.

CONCEPTUAL MODEL

The conceptual model of the East Mesa geothermal system is shown in Figure 6. The basement complex of granite-metamorphic rocks is at a depth of about 4 km from the surface [Combs and Hadley, 1977]. The

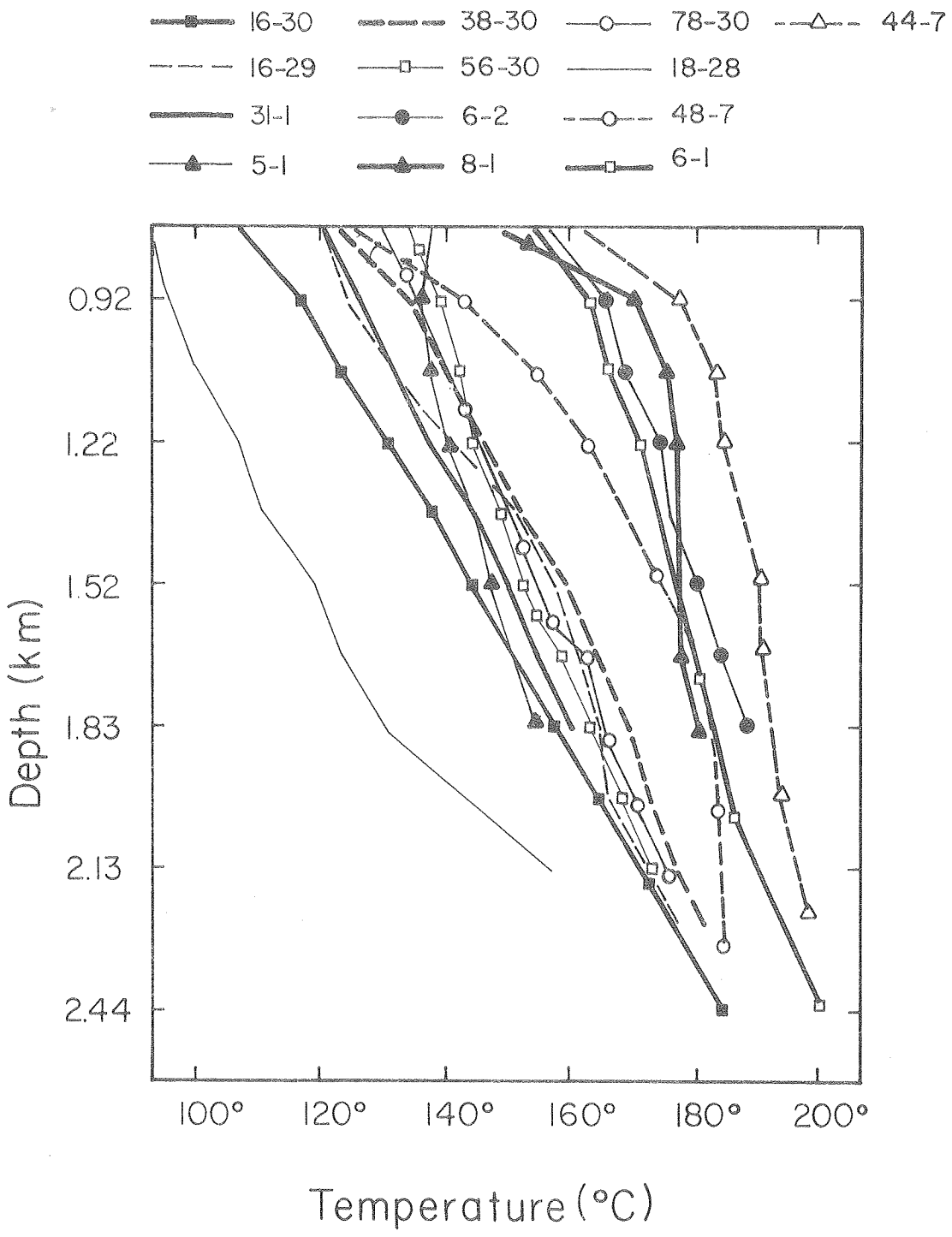

Figure 5. Temperature-depth profile for East Mesa wells below 800 meters depth.

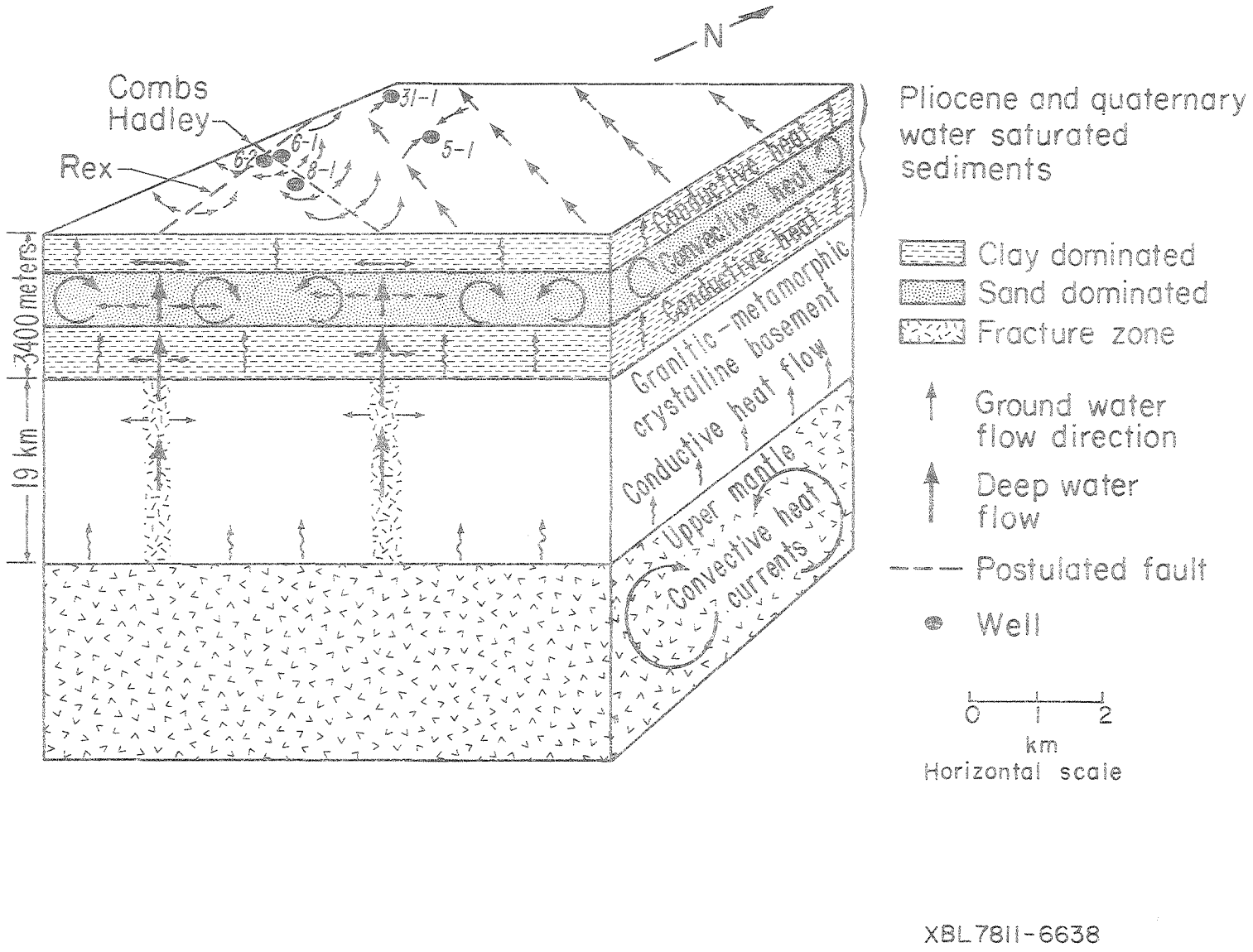

Figure 6. Conceptual model of the East Mesa anomaly. (Adapted from Bailey, [1977].)

basement complex is subjected to failure under adequate stresses. Fractures, once formed, would tend to be preserved in this high-strength rock. Nearly vertical tension fractures probably were the first to form during the evolution of the Salton Trough. These fractures would increase the vertical permeability much more than the horizontal permeability.

A shale-dominated zone overlies the basement. It is characterized by (1) steepening of the temperature profile in Mesa Well 6-1 below about 2100 meters depth, (2) an increase in percentage of shale and corresponding decrease in sands below 2200 m depth, and (3) marked change in salinities below 2200 m depth [Black, 1975]. This layer extends from the basement complex to about 1900-2200 m from the surface. Here the sediments are indurated by overburden and heat. They probably fracture, given any movement on the basement faults. The vertical permeability of these sediments is expected to be good near the fracture, but quite low away from it. The horizontal permeability in this layer is also thought to be only moderate because of the presence of clay and dirty sands.

Sands dominate the sedimentary zone from about 800 to 1900 m depth. Horizontal permeability in this zone is probably better than in the underlying material because of greater sand content and continuity and less compaction. Vertical permeability should be good near the fracture zones and in general should be better than in the underlying beds because of the greater amount of sand. Except near the fracture zones, relatively fresh water in this sand-dominated zone may be prevented from extensive mixing with more saline water in the sediments below by the restricted vertical permeability of the sediments in the lower zone.

The next 600 m or so of the sediments are dominated by clay. Fractures may form temporarily in these sediments with sudden differential motion, but under light loading, fractures in these beds would tend to close by slow flowage unless there are repeated fast movements. The vertical permeability is probably very low in these young sediments, but the numerous shallow wells in them indicate that their horizontal permeability is good.

The upper 200 m of the valley fill appears to have more sand and better porosity than the underlying zone. Vertical permeability is probably much higher than in the underlying zone. However, this zone and the underlying clay-dominated zone probably behave in similar ways when subjected to stress.

In summary, what vertical permeability exists in the lower four zones is due almost entirely to fractures, whereas, except in the vicinity of a fracture, horizontal flow in these zones is largely dependent upon intergranular permeability. The major source of fluid for southern Imperial Valley brines is the underflow from the Colorado River. This water percolates gradually into sediments and/or fractured basement rock over an area considerably larger than the anomaly itself. Heated at depth by an as yet undefined source, the liquid can rise in the high permeability fractured fault zone, convecting energy towards the surface. When a horizontal aquifer of relatively large permeability is intersected, reservoir charging will occur.

MATHEMATICAL MODEL

The relative positions of the heat flux contours about the Mesa fault (Figure 2) tell us that the hot water rises up the fault and then spreads laterally losing heat to the surroundings. This idea is also

confirmed by the location of the charging plane A in Figure 4. If we consider a vertical front view at Section AA' of Figure 2, a two dimensional vertical model such as that given in Figure 7 would result. In this model, we have combined the upper two zones to represent a clay cap and the lower two zones to represent an aquifer. The fault is hypothesized to be a vertically oriented region of heavily fractured material of finite width ($2y_e'$). The vertical extent of the fault and its second horizontal dimension are large compared to its width. The fault extends downward through the clay-rich region (cap) of thickness ℓ', through the interbedded sediments of the reservoir for a distance L', and finally into the basement rock. It is postulated that the fault is charged at depth by liquid that has been heated in an extensive basement fractured system. The rate of charge cannot be obtained a priori without a global analysis of the entire convection process. The liquid rises up in the reservoir section of the fault. The presence of clays in the cap suppresses the vertical transport there. Water pushed out of the fault by the overpressure associated with convection is assumed to flow horizontally in the aquifer. The vertical transport should be less important, in large because of the presence of shaley layers associated with interbedding.

For mathematical purposes, the fracture zone is idealized as a vertical slab of porous medium. The adjacent aquifer is represented as a porous medium of lateral half width H' with horizontal permeability much larger than a vertical value of small absolute magnitude. The overlying clay cap is assumed to be impermeable. Spatially uniform temperature boundary conditions are imposed on the cold cap surface and at the hot

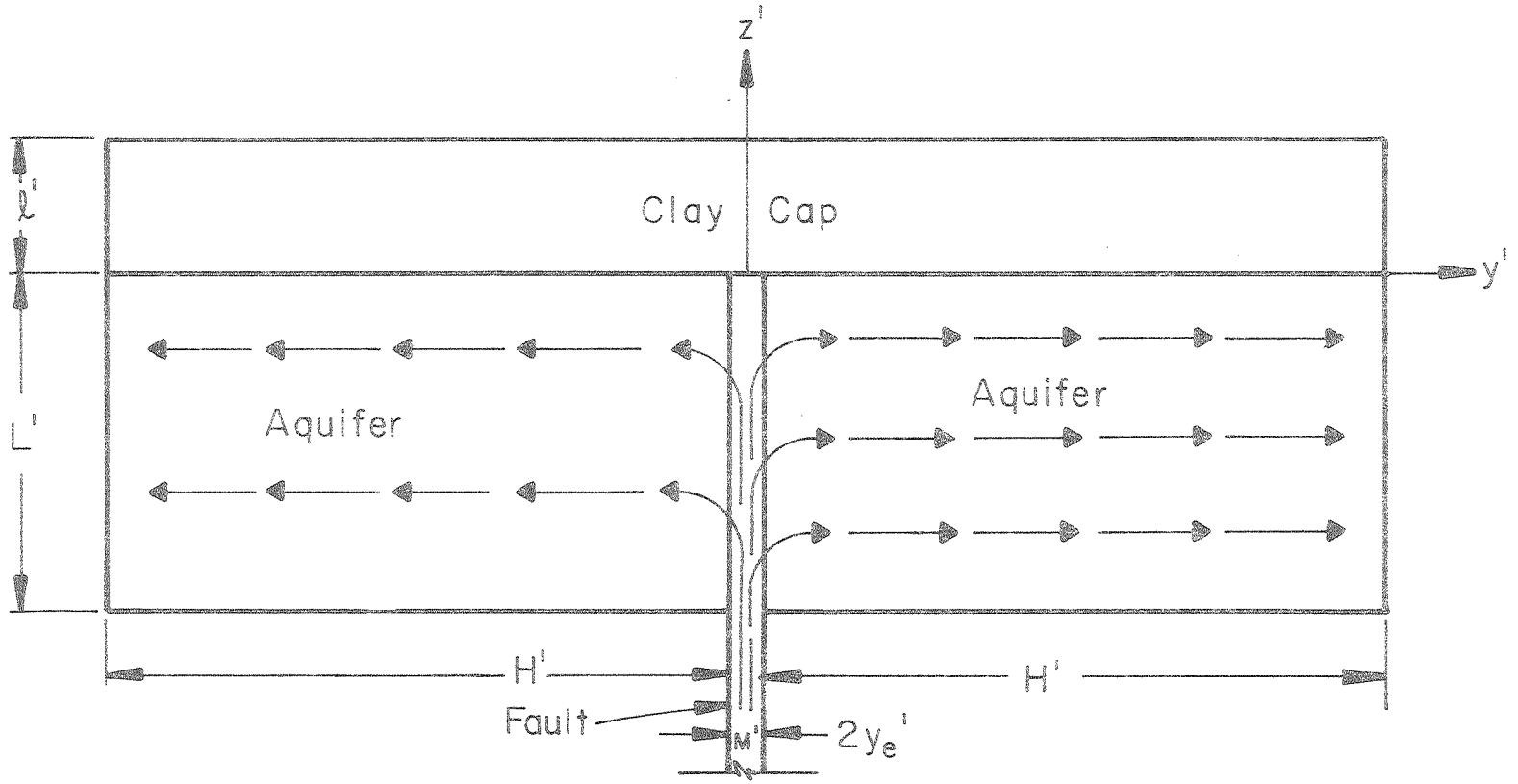

XBL 7811-6631

Figure 7. A two-dimensional mathematical model of the East Mesa anomaly.

bottom boundary of the reservoir. On the lateral boundary far from the fault ($H' >> L' >> y_e'$) the temperature distribution is assumed to be controlled by vertical conduction. The associated pressure distribution can be found once the density distribution is calculated. Finally, a horizontal mass flux is permitted in order to conserve matter.

A quasi-analytic theory is developed for high Rayleigh number convection of a liquid in a rigid porous medium. In this approximation liquid rises up the fault and spreads into the near regions of the reservoir adiabatically. The cooling effect of the cap in the reservoir is confined to a thin layer adjacent to the interface. The layer grows with distance from the fault. In the far field of the aquifer, the full depth of the reservoir is cooled by the surface.

A detailed derivation of the describing equations for a thermally active, saturated, and deformable porous material is given in Goyal [1978]. The equations used here are obtained from that set by assuming that the flow is steady, the solid matrix is rigid, the fault medium is homogeneous and isotropic, liquid properties (except density) are constant, the thermal conductivities of the fault and aquifer media are constant and equal, the clay cap is impermeable, and that the vertical permeability in the aquifer is much smaller than the horizontal value, which is equal to that of the fault. Thus for all practical purposes vertical velocity in the aquifer is nearly zero. In addition, the Boussinesq approximation is invoked. The describing dimensional equations are:

Fault zone:

$$V'_{y'} + W'_{z'} = 0 \qquad (1)$$

$$V' = -\frac{K'}{\nu'} P'_{y'} \tag{2}$$

$$W' = \frac{K'}{\nu'} \{-(P' - P'_H)_{z'} + g'(\rho' - \rho'_o)\} \tag{3}$$

$$C'_p \{V' T'_{y'} + W' T'_{z'}\} = \lambda'_m \{T'_{y'y'} + T'_{z'z'}\} \tag{4}$$

$$\rho' = \rho'_o \left[1 - \alpha'_e (T' - T'_o)\right] \tag{5}$$

Aquifer:

$$v'(z') = -\frac{K'}{\nu'} p'_{y'} \tag{6}$$

$$C'_p v' \theta'_{y'} = \lambda'_m (\theta'_{y'y'} + \theta'_{z'z'}) \tag{7}$$

Clay Cap:

$$\theta^{C'}_{y'y'} + \theta^{C'}_{z'z'} = 0 \tag{8}$$

where the variables are defined following equation (25). The solution of the above system is subjected to the following boundary and continuity conditions.

Boundary Conditions:

Fault Zone

$$W'(y',0) = 0 \qquad \text{impermeable upper boundary} \tag{9}$$

$$\int_{-y_{e'}}^{+y_{e'}} W'(y', -L')\, dy' = M', \qquad \text{input mass flow rate} \tag{10}$$

$$T'(y', -L') = T'_{max}, \qquad \text{hot lower boundary} \tag{11}$$

$$T'_{y'}(0,z') = 0, \qquad \text{symmetry} \tag{12}$$

Aquifer:

$$\theta'(y', -L') = T'_{max}, \qquad \text{hot lower boundary} \tag{13}$$

$$\theta'(H', z') = T'_{ac} - (T'_{max} - T'_{ac}) \frac{z'}{L'}, \quad -L' \leq z' \leq 0, \quad \text{aquifer edge} \tag{14}$$

where T'_{ac} is the aquifer-clay cap interface temperature at the far field boundary and can be expressed as:

$$T'_{ac} = \frac{\lambda'_m \ell' T'_{max} + \lambda^{c'}_m L' T'_o}{\ell' \lambda_{m'} + L' \lambda^{c'}_m} \tag{15}$$

Clay Cap:

$$\theta^{c'}(y', \ell') = T'_o, \qquad \text{cold upper boundary} \tag{16}$$

$$\theta^{c'}_{y'}(0,z') = 0, \qquad \text{symmetry} \tag{17}$$

$$\theta^{c'}(H', z') = T'_{ac} - (T'_{ac} - T'_o) \frac{z'}{\ell'}, \quad 0 \leq z' \leq \ell', \quad \text{clay cap edge} \tag{18}$$

Continuity Conditions at the Fault-Aquifer Boundary:

$$T'(y'_e, z') = \theta'(y'_e, z') \tag{19}$$

$$V'(\pm y'_e, z') = \pm v'(z') \tag{20}$$

$$P'(y_e', z') = p'(y_e', z') \tag{21}$$

Continuity Conditions at the Fault-Clay Cap Boundary:

$$T'(y', 0) = \theta^{c'}(y', 0), \tag{22}$$

$$\lambda_m' T_{z'}'(y', 0) = \lambda_m^{c'} \theta_{z'}^{c'}(y', 0) \tag{23}$$

Continuity Conditions at the Aquifer-Clay Cap Boundary:

$$\theta'(y', 0) = \theta^{c'}(y', 0) \tag{24}$$

$$\lambda_m' \theta_{z'}'(y', 0) = \lambda_m^{c'} \theta_{z'}^{c'}(y', 0) \tag{25}$$

The dimensional variables are defined by:

V' = horizontal Darcy mass flux in the fault per unit area, gm/cm^2-sec

W' = vertical Darcy mass flux in the fault per unit area, gm/cm^2-sec

K' = fault permeability and horizontal permeability in the aquifer, cm^2

ν' = kinematic viscosity, cm^2/sec

P' = fault pressure, $dynes/cm^2$

P_H' = cold hydrostatic pressure with respect to density ρ_o', $dynes/cm^2$

ρ_o' = density of the liquid at the ambient temperature T_o', gm/cm^3

ρ' = density of the liquid at the temperature T', gm/cm^3.

g' = acceleration due to gravity, cm/sec^2

C_p' = specific heat of the liquid at constant pressure, cm^2/sec^2- ^oK

T' = fault temperature, ^oK

λ_m' = medium thermal conductivity of the fault and the aquifer, $gm\text{-}cm/sec^3\text{-}^oK$

α_e' = coefficient of thermal expansion of the liquid,/^oK.

T_o' = ambient temperature, ^oK

v' = horizontal Darcy mass flux in the aquifer per unit area, gm/cm^2-sec

p' = aquifer pressure, $dynes/cm^2$

θ' = aquifer temperature, ^oK

$\theta^{c'}$ = clay cap temperature, ^oK

y_e' = semifault width, cm

L' = depth of the reservoir, cm

M' = mass flow rate per unit length in the direction perpendicular to the plane of paper, gm/cm-sec.

T'_{max} = maximum temperature at the hot bottom boundary of the reservoir, ^oK

H' = width of the aquifer in the y'-direction, cm

ℓ' = thickness of the clay cap, cm

$\lambda_m^{c'}$ = medium thermal conductivity of the clay cap, $gm\text{-}cm/sec^3\text{-}^oK$.

In the fault, where the characteristic horizontal dimension and velocity component are much smaller than their vertical counterpart, the appropriate nondimensional variables can be defined as:

$$\bar{y} = y'/y_e', \quad y_e = y_e'/L', \quad z = z'/L'$$

$$\bar{V} = V'/y_e\, q_o'\, \rho_o', \quad W = W'/q_o'\, \rho_o', \quad T = T'/T_o' \tag{26}$$

$$\tau = (T'_{max} - T_o')/T_o', \quad P = (P' - P_H')/P_o'$$

Substitution of (26) into (1) to (5) leads to an inherent balance between the buoyancy, Darcy and pressure terms in the vertical momentum equation, if

$$q_o' = \frac{\alpha_e' \Delta T' g' K'}{\nu'} = \text{reference convection velocity}$$

$$p_o' = \rho_o' g' \alpha_e' L' \Delta T' = \text{reference convection pressure}$$

$$R = \frac{\rho_o' q_o' C_p' \Delta T'}{\lambda_m' (\Delta T'/L')} = \text{Rayleigh number} \qquad (27)$$

where $\Delta T' = T'_{max} - T'_o$

The non-dimensional equations, transformed boundary and continuity conditions relevant in the fault zone can be written as:

Fault Zone:

$$\bar{V}_{\bar{y}} + W_z = 0 \qquad (28)$$

$$y_e^2 \bar{V} = - P_{\bar{y}} \qquad (29)$$

$$W = - P_z + (T-1)/\tau \qquad (30)$$

$$\gamma^2(\bar{V}T_{\bar{y}} + WT_z) = T_{\bar{y}\bar{y}} + y_e^2 T_{zz} \qquad (31)$$

$$\gamma = y_e R^{\frac{1}{2}} \qquad (32)$$

$$W(\bar{y},0) = 0 \qquad (33)$$

$$W(\bar{y},-1) = M \qquad (34)$$

$$M = M'/M_o' \ , \ M_o' = 2y_e' \rho_o' q_o' \qquad (35a,b)$$

$$T(\bar{y},-1) = 1+\tau \qquad (36)$$

$$T_{\bar{y}}(0,z) = 0 \qquad (37)$$

$$T(\bar{y},0) = \theta^c(\bar{y},0) \qquad (38)$$

$$T_z(\bar{y},0) = \lambda\theta^c_z(\bar{y},0) \tag{39}$$

$$V(\pm 1,z) = \pm v(z) \tag{40}$$

where λ is the ratio of the thermal conductivities of the cap and the aquifer. Equations (38) and (39) represent the continuity of temperature and heat flux at the boundary between clay cap and fault. In the aquifer, where the horizontal scale is measured by $\hat{y} = y'/H'$, the pressure $p = P$, the temperature $\theta = T$, and the velocity $v = V$, the appropriate system of equations is given by:

Aquifer:

$$v(z) = -p_{\hat{y}}/d \tag{41}$$

$$d\gamma^2 v(z)\theta_{\hat{y}} = y_e{}^2\theta_{\hat{y}\hat{y}} + d^2\theta_{zz} \tag{42}$$

where

$$H'/L' = d/y_e, \quad d = O(1) \text{ number} \tag{43a,b}$$

The magnitude of H' with respect to the fault depth L' in (43) is chosen to ensure a balance between the nondimensional aquifer velocity v and the horizontal pressure gradient shown in (41). The number d, used in this study to define the location of the far-field boundary of the aquifer, will be determined by finding a location where the horizontal temperature gradient in the aquifer becomes vanishingly small. It may be emphasized that the horizontal motion exists at the far field boundary but the heat transfer is due to vertical conduction only. The nondimensional boundary and continuity conditions for the aquifer are:

$$\theta(\hat{y},0) = \theta^c(\hat{y},0) \tag{44}$$

$$\theta_z(\hat{y},0) = \lambda\theta^c_z(\hat{y},0) \tag{45}$$

$$\theta(\hat{y},-1) = 1+\tau \tag{46}$$

$$\theta\left(\hat{y} = \frac{y_e^2}{d}\ ,\ z\right) = T(\bar{y} = 1,\ z) \tag{47}$$

$$\theta(\hat{y} = 1,z) = 1 + \frac{\tau}{\lambda+\ell}\ (\ell - \lambda z),\ -1 \leq z \leq 0 \tag{48}$$

where $\ell = \ell'/L'$. Equations (44) and (45) represent the continuity of the temperature and the heat flux at the interface between the aquifer and the clay cap.

In the clay cap, where the temperature $\theta^c = \theta^{c'}/T'_o$, the energy equation, boundary, and continuity conditions are as follows:

$$y_e^2\ \theta^c_{\hat{y}\hat{y}} + d^2\theta^c_{zz} = 0 \tag{49}$$

$$\theta^c(\hat{y},\ell) = 1 \tag{50}$$

$$\theta^c_{\hat{y}}\ (0,z) = 0 \tag{51}$$

$$\theta^c(1,z) = 1 + \frac{\tau}{\lambda+\ell}\ (\ell-z),\ 0 \leq z \leq \ell \tag{52}$$

Temperature and heat flux continuity conditions between the fault and clay cap and also between aquifer and clay cap interfaces are already expressed in equations (38), (39), (44) and (45).

In order to proceed further we must consider the magnitude of the Rayleigh number and the parameter γ associated with the East Mesa anomaly. The depth of the basement in this anomaly is about 4.15 km [Combs, 1977]. From well logs, one can assume the thickness of the clay cap (ℓ') to be 0.8 km. Thus the reservoir thickness (L'), consisting of both low and high permeability zones, equals to 3.35 km. The ratio (ℓ) of cap thickness (ℓ')

to the reservoir depth (L′) is thus equal to 0.238. The formation temperatures, based on Na-K-Ca geothermometry, are about 200°C ± 30°C [Bailey, 1977]. If the formation temperature (T'_{max}) is assumed to be 200°C, we find that the maximum temperature difference ($\Delta T'$) across the system is 175°C and the overheat ratio (τ) is 0.587. The thermal conductivity of a geothermal reservoir depends on many factors such as its porosity, grain size, size distribution, physical properties of rocks and fluids, fluid saturation, temperature, and pressure. In the laboratory, the thermal conductivity of rock samples is found to increase with increasing liquid saturation [Somerton et al., 1974] and decreases with increasing temperatures [Martinez-Baez, 1978]. The thermal conductivities of the saturated sand stones were found to vary between 4×10^{-3} to 6.4×10^{-3} cal/cm-sec-°K in the Cerro Prieto geothermal field, Mexico [Martinez-Baez, 1978]. Besides being less than 50 km apart, East Mesa and Cerro Prieto fields both lie in the Colorado River delta stratigraphic system. Thus the physical properties of the sediments in the two systems are not expected to vary much and so we assume an average thermal conductivity (λ'_m) value of 4.91×10^{-3} cal/cm-sec-°K for the reservoir part of the East Mesa system. Measured thermal conductivity values of unconsolidated sands, silts and clays in the upper 40 to 150 meters range from 2.48×10^{-3} to 3.88×10^{-3} cal/cm-sec-°K [Combs, 1972]. Thus an average thermal conductivity ($\lambda^{c,}_m$) of 3.44×10^{-3} cal/cm-sec-°K is assumed for the clay cap of the East Mesa system. This data leads to a thermal conductivity ratio (λ) of 0.7.

The permeability values obtained from the log analysis for the Republic geothermal wells ranged from 68.8 md to 941.3 md at a depth interval of 1524 m to 2134 m [Smith, 1979]. A drastic decrease in the permeability values was noted below this depth interval. Based on well test analysis, the permeabilities of the USBR wells ranged from 30 md to 84 md [Howard et al., 1978]. Thus we have assumed a representative value of 100 md ($K' = 10^{-9} cm^2$) for the permeability in the East Mesa area. If the thermodynamic variables evaluated at $T'_o = 298^oK$ are used in (27) and (35b) we find that

$q'_o = 0.43$ cm/day

$p'_o = 14.7$ atm

$R = 338.$

For a fault width of 230 m, as calculated later in this paper, we find from (35b) that $M_o' = 9.89 \times 10^5$ kg/day-km.

The local values of the above parameters may be 10 to 20 times higher if the local values of the physical properties are used. The Rayleigh number is also sensitive to the changes in permeability. The large values of R suggest that the energy transfer associated with liquid convection is far greater than that due to conduction. In this regard one may expect that fluid particles moving through the system will tend to behave isothermally unless affected by cooling associated with a relatively cold boundary.

It is possible to calculate the fault width based on energy transfer considerations as follows:

energy convected upward in the fault, per unit area $E'_{conv} = \rho' q'_o e'$

where e′ is the internal energy of the liquid flowing in the fault. For an average temperature of 200°C in the fault, the convected energy is about 10^7 cal/sec-km^2. In contrast, for a normal temperature gradient of 30°C/km, heat conducted through the clay cap is about 10^4 cal/sec-km^2. Thus the convected energy is about 3 orders of magnitude larger than the purely conductive flux. The temperature drop experienced by the fluid in moving from Mesa well 6-2 to 5-1 is about 10% in the convection-dominated zone (Figure 5). Thus for a 10% energy loss to the surroundings, total heat lost through the cap is equal to $A_F' \times 10^6$ cal/sec where A_F' is the area of fault in km^2. This quantity, when measured from the contours of Figure 2 is 4.88 x 10^6 cal/sec crossing an area of 110 km^2. Upon equating these quantities, one can then obtain the horizontal fault zone area (A_F') of 4.88 km^2. Since the thermal activity of the Mesa field extends along the primary fault for about 21 km, a fault (fracture zone) width ($2y_e'$) of 230 m is suggested. Morrison et al. [1979] came up with a fault width of 300 to 600 m based on their self potential study. It may be noted that the Mesa well 44-7, located at the intersection of the Rex and Babcock faults (Figure 2) is the hottest in the field (Figure 5). This suggests that the Mesa fault is not the only fault contributing to this anomaly. Thus one should recognize that the suggested fault width is an order-of-magnitude estimate. Given the variable nature of input, a range 50 m $\leq y_e' \leq$ 150 m might be appropriate. If the characteristic permeability were far smaller than 10^{-9} cm^2, the fault zone area estimate would be far larger and thus not representative of the relatively localized anomalous properties of the Mesa field.

The parameter γ is assumed to be an O(1) number because y_e is considered small. For instance, a value of 0.034 is obtained for y_e and 0.63

for γ if the previously discussed data of East Mesa is used. In the mathematical analysis, solutions are sought in the limit of large R with $\gamma = O(1)$, implying, of course, that y_e is small.

Above the fault the cooling effect of the cap is confined to a thin thermal-boundary layer adjacent to the cap-fault interface, for a high Rayleigh number flow. The cooled boundary layer thickness increases as the fluid moves horizontally away from the fault. Beneath the boundary layer, the flow is isothermal. In the far field, the surface cooling effect influences the temperature distribution throughout the aquifer depth.

It can be noted from (29) that the horizontal pressure gradient in the fault is very small, $O(y_e^2)$. Thus the basic fault pressure is only a function of depth and can be calculated in terms of W or v. The horizontal aquifer velocity distribution v(z) can then be calculated explicitly from (41) because far-field pressure is known once (14) and (18) are specified. Upon decoupling the fluid mechanics from the thermal problem, the energy equations (42) and (49) can be solved for temperatures in the aquifer and the clay cap respectively, ensuring the continuity of the temperature and heat flux at the interface. To determine the temperatures, the fault aquifer system is divided into seven regions as shown in Figure 8. The solution procedure is similar to that used in Coyal and Kassoy [1980] to describe the capless system.

First we obtain the basic temperatures in the fault and near fault regions of the aquifer (regions 1 to 4). With the interface temperatures known, we then calculate the lowest-order temperatures in region 6 of the clay cap. To ensure the continuity of the heat flux at the interface, we then calculate the boundary layer temperature corrections in regions 1 and 3.

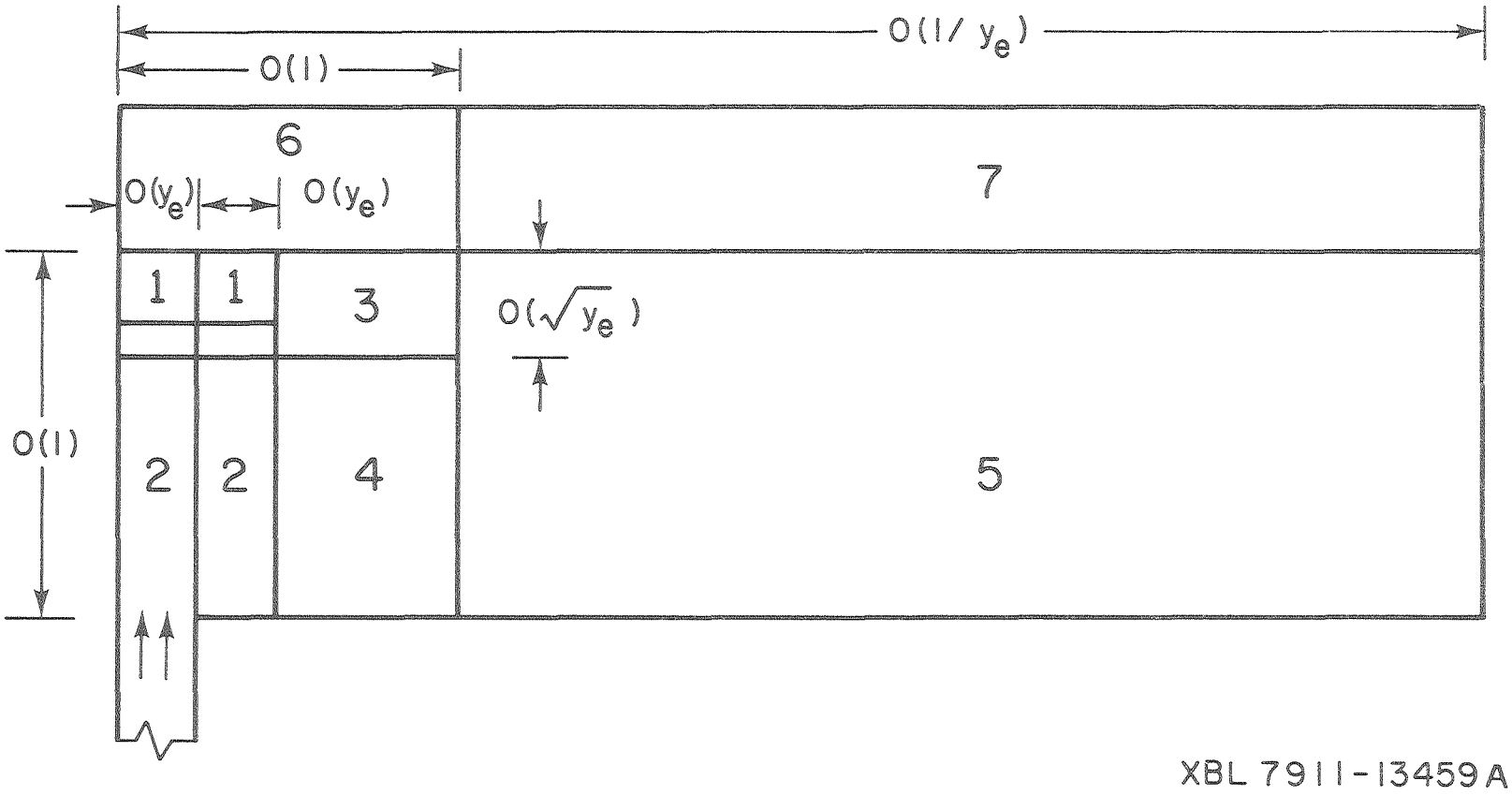

Figure 8. Seven different regions in the fault-aquifer system.

Temperatures in regions 5 and 7 are subsequently obtained for $\hat{y} \rightarrow 0$. With these known initial conditions, equations (42) and (49) are solved numerically in regions 5 and 7 for continuous heat flux and temperature at the interface.

FAULT ZONE SOLUTION

The presence of the clay cap over the fault-aquifer system acts as an insulator that reduces the heat transfer to the surface relative to a capless system. The basic temperature of the hot liquid rising in the fault at a high Rayleigh number will remain at the supply temperature. Since the cooling can occur only through the cap, the lowest order temperatures in regions 1,2,3 and 4 of the aquifer are also expected to be equal to that in the fault. Once the temperatures in the fault zone are known, solutions for pressures and velocities in the fault and aquifer are calculated in a manner similar to Goyal and Kassoy [1980]. In this case equations (29) and (30) are solved to obtain a relation between W and P to the lowest order. It turns out that to this order both P and W are functions of z only. A relation between aquifer velocity v and vertical fault velocity W can be obtained from the mass conservation equation (28). Finally, equations (41) and (48) can be used to determine a relation between fault pressure P and aquifer velocity v. It can be noted that equation (48) is used to determine the hydrostatic pressure at the far-field boundary of the field. Three relations thus obtained, can be used to form a second order ordinary differential equation in terms of W, and the equation can then be solved for boundary conditions (33) and (34). Once W is known, P and v can then be obtained from the relations mentioned above.

The basic solutions of the fault-aquifer system are:

$$T = 1 + \tau \tag{53}$$

$$\bar{V} = \bar{y}\left\{ a_2 \cosh \frac{z}{\sqrt{d}} + b_2 \sinh \frac{z}{\sqrt{d}} - \frac{\lambda}{\lambda+\ell} \right\} + O(y_e^2) \tag{54}$$

$$W = -a_2\sqrt{d} \sinh \frac{z}{\sqrt{d}} + b_2 \sqrt{d}\left(1 - \cosh \frac{z}{\sqrt{d}}\right) + \frac{\lambda z}{\lambda+\ell} + O(y_e^2) \tag{55}$$

$$P = d\left\{ a_2 \cosh \frac{z}{\sqrt{d}} + b_2 \sinh \frac{z}{\sqrt{d}} - \frac{\lambda}{\lambda+\ell} \right\} - \frac{\ell^2 - 2\ell z + \lambda z^2}{2(\lambda+\ell)} + O(y_e^2) \tag{56}$$

$$v(z) = a_2 \cosh \frac{z}{\sqrt{d}} + b_2 \sinh \frac{z}{\sqrt{d}} - \frac{\lambda}{\lambda+\ell} + O(y_e^2) \tag{57}$$

$$p = v(z)d(1-\hat{y}) - \frac{\ell^2 - 2\ell z + \lambda z^2}{2(\lambda+\ell)} + O(y_e^2) \tag{58}$$

where

$$a_2 = \frac{M + \frac{\lambda}{\lambda+\ell} \cosh \frac{1}{\sqrt{d}}}{\sqrt{d} \sinh \frac{1}{\sqrt{d}}}, \quad b_2 = \frac{\lambda}{\sqrt{d}(\lambda+\ell)} \tag{59a,b}$$

It may be noted that $\left(- \frac{\ell^2 - 2\ell z + \lambda z^2}{2\lambda + 2\ell}\right)$ represents the pressure at the far field boundary of the aquifer and is consistent with the specified temperature field (48). It may also be observed that the temperatures given by (53) are only valid in regions 2 and 4 of figure 8. Once the fault temperature is known, one can calculate the basic temperatures in region 6 of the clay cap from the system of equations (91) to (95). The result is given by (96). The continuity of heat flux at the horizontal interface between the fault and the clay cap implies the necessity of a thermal boundary layer near the top of the fault. If the appropriately scaled variables

$$\bar{z} = \frac{z}{y_e} \quad \text{and} \quad \bar{W} = \frac{W}{y_e} \tag{60a,b}$$

are used in the basic fault-zone equations then the lowest order boundary layer system has the form:

$$\bar{V}_{o\bar{y}} + \bar{W}_{o\bar{z}} = 0 \tag{61}$$

$$P_{1\bar{y}} = 0 \tag{62}$$

$$\frac{T_o - 1}{\tau} - P_{1\bar{z}} = 0 \tag{63}$$

$$\gamma^2\left(\bar{V}_o T_{o\bar{y}} + \bar{W}_o T_{o\bar{z}}\right) = T_{o\bar{y}\bar{y}} + T_{o\bar{z}\bar{z}} \tag{64}$$

However, it can be seen that the lowest order fault temperature T_o and pressure P_o are constant and when matched with the outer solutions (53) and (56) one finds that

$$T_o = 1 + \tau \tag{65}$$

$$P_o = d\left(a_2 - \frac{\lambda}{\lambda+\ell}\right) - \frac{\ell^2}{2(\lambda+\ell)} \tag{66}$$

Equation (65) satisfies the energy equation (64) identically. The solution to the system of equations (61) to (63) is subjected to the following boundary, matching, and continuity conditions.

$$\bar{V}_o(\pm 1, \bar{z}) = \pm v_o(\bar{z}) \quad \text{[equation (84)]} \tag{67}$$

$$\bar{W}_o(\bar{y}, \bar{z} \to -\infty) = -\left(a_2 - \frac{\lambda}{\lambda+\ell}\right)\bar{z} \tag{68}$$

$$P_1(\bar{y}, \bar{z} \to -\infty) = \bar{z} \tag{69}$$

It may be noted that the matching conditions ($\bar{z} \to -\infty$) are obtained from the outer solutions (55) and (56) respectively. The solutions to this system for all values of $\bar{y}$ and $\bar{z}$ are equal to those expressed by the matching conditions (67) to (69). This occurs because the boundary layer is required to smooth a discontinuous derivative of T rather than the function itself. The describing system for the $0(y_e)$ terms is

$$\bar{V}_{1\bar{y}} + \bar{W}_{1\bar{z}} = 0 \tag{70}$$

$$-\gamma^2 \left(a_2 - \frac{\lambda}{\lambda+\ell}\right) \bar{z} \frac{dT_1}{d\bar{z}} = \frac{d^2T_1}{d\bar{z}^2} \tag{71}$$

The momentum equations in y and z directions can be used to show that T_1 is only a function of $\bar{z}$. The associated matching and boundary conditions for the system of equations (70) and (71) are

$$\bar{V}_1 (\pm 1, \bar{z}) = \pm v_1(\bar{z}) \qquad \text{[equation (89)]} \tag{72}$$

$$\bar{W}_1(\bar{y}, \bar{z} \to -\infty) = -\frac{b_2 \bar{z}^2}{2\sqrt{d}} \tag{73}$$

$$\frac{dT_1}{d\bar{z}} (\bar{y}, 0) = -\frac{\tau\lambda}{\ell} \qquad \text{[equation (96)]} \tag{74}$$

$$T_1(\bar{y}, \bar{z} \to -\infty) = 0 \tag{75}$$

It may be noted that (74) implies continuity of heat flux at the horizontal interface between fault and clay cap. The solutions to the system (70) to (75), when added to 0(1) solutions (65) to (69) form the complete solutions for the boundary layer, as follows:

$$\bar{V} = \left(a_2 - \frac{\lambda}{\lambda+\ell}\right)\bar{y} + y_e \frac{b_2 \bar{y}\bar{z}}{\sqrt{d}} + O(y_e^2) \tag{76}$$

$$\bar{W} = -\left(a_2 - \frac{\lambda}{\lambda+\ell}\right)\bar{z} - y_e \frac{b_2 \bar{z}^2}{2\sqrt{d}} + O(y_e^2) \tag{77}$$

$$P = d\left(a_2 - \frac{\lambda}{\lambda+\ell}\right) - \frac{\ell^2}{2(\lambda+\ell)} + y_e\,\bar{z} + O(y_e^2) \tag{78}$$

$$T = 1 + \tau - ye\,\frac{\sqrt{\Pi\tau\lambda}}{2B\ell}\left[1 + \mathrm{erf}(B\bar{z})\right] + O(y_e^2) \tag{79}$$

where

$$B = \sqrt{\frac{\gamma^2}{2}\left(a_2 - \frac{\lambda}{\lambda+\ell}\right)} \tag{80}$$

The thermal boundary layer initiated at the top of the fault continues into the adjacent aquifer over a horizontal distance to scale y_e'. In this initial aquifer zone of water cooling, the relevant lowest order equation for the velocity and pressure field is

$$v_o(\bar{z}) = -\frac{p_{o\hat{y}}}{d} \tag{81}$$

the appropriate boundary and continuity conditions are

$$p_o(\hat{y} \to 0, \bar{z}) = P_o(\bar{y} = 1, \bar{z}) = d\left(a_2 - \frac{\lambda}{\lambda+\ell}\right) - \frac{\ell^2}{2(\lambda+\ell)} \quad \text{[equation (66)]} \tag{82}$$

$$p_o(1,\bar{z}) = -\frac{\ell^2}{2(\lambda+\ell)} \tag{83}$$

The solution forms are

$$v_o(\bar{z}) = \left(a_2 - \frac{\lambda}{\lambda+\ell}\right) \tag{84}$$

$$p_o(\hat{y},\bar{z}) = (1-\hat{y})d\left(a_2 - \frac{\lambda}{\lambda+\ell}\right) - \frac{\ell^2}{2(\lambda+\ell)} \tag{85}$$

The aquifer momentum equation, describing $0(y_e)$ terms is

$$v_1(\bar{z}) = -\frac{p_{1\hat{y}}}{d} \tag{86}$$

The appropriate boundary and continuity conditions are

$$p_1(\hat{y} \to 0,\bar{z}) = p_1(\bar{y} = 1,\bar{z}) = \bar{z} \text{ , [from equation (69)]} \tag{87}$$

$$p_1(\hat{y} = 1,\bar{z}) = \frac{\ell\bar{z}}{(\lambda+\ell)} \tag{88}$$

The solutions to the system (86) to (88) when added to 0(1) solutions (84) and (85) give the following complete solutions in the aquifer boundary layer.

$$v(\bar{z}) = \left(a_2 - \frac{\lambda}{\lambda+\ell}\right) + y_e \frac{b_2}{\sqrt{d}}\bar{z} + 0(y_e^2) \tag{89}$$

$$p(\hat{y},\bar{z}) = d\left(a_2 - \frac{\lambda}{\lambda+\ell}\right)(1-\hat{y}) - \frac{\ell^2}{2(\lambda+\ell)} + y_e\left[b_2\sqrt{d}\,\bar{z}\,(1-\hat{y}) + \frac{\ell\bar{z}}{\lambda+\ell}\right] + 0(y_e^2) \tag{90}$$

It is observed that the boundary layer solutions [equations (89) and (90)] match with the outer solutions [equations (57) and (58)].

TEMPERATURES IN THE CLAY CAP

The lowest-order energy equation, in the region 6 where the length scale is of $O(L')$, is given as follows:

$$\theta^c_{oyy} + \theta^c_{ozz} = 0 \tag{91}$$

where $y = y'/L'$ (92)

The appropriate boundary conditions are;

$$\theta^c_{oy}\ (0,z) = 0 \quad , \qquad \text{symmetry} \tag{93}$$

$$\theta^c_o\ (y,\ell) = 1 \quad , \qquad \text{cold top boundary} \tag{94}$$

$$\theta^c_o\ (y,0) = 1 + \tau, \qquad y = 0\ (1)\ , \quad \text{bottom boundary} \tag{95}$$

where

$\theta^c_o\ (y \to \infty, z)$ is well behaved.

The symmmetry condition in (93) implies that the complete temperature solution is given by the elementary form,

$$\theta^c_o\ (z) = 1 + \tau\left(1 - \frac{z}{\ell}\right) \tag{96}$$

The higher-order temperature distributions in the clay cap above the fault can be calculated in a manner similar to equations (91) to (96) if the higher-order interface temperatures are known. The interface temperature between clay cap and fault can be obtained from $O(y_e)$ terms of equation (79). The temperature solution in the clay cap for $|\bar{y}| \leq 1$ is given as follows,

$$\theta^c(y,z) = 1 + \tau\ \left(1 - \frac{z}{\ell}\right) - y_e \frac{\sqrt{\Pi\tau\lambda}}{2B\ell}\ \left(1-\frac{z}{\ell}\right) + O(y_e{}^2) \tag{97}$$

The temperature in region 6 of the clay cap for all values of y, which is compatible with that in region 3 of the aquifer, can be written as:

$$\theta^c(y,z) = 1+\tau\left(1 - \frac{z}{\ell}\right) + y_e^{1/2}\sqrt{\frac{2}{\Pi}}\frac{\tau\lambda}{B\ell}\,\theta_1^c\,(y,z) + 0(y_e) \tag{98}$$

where θ_1^c is given by following Laplace equation and boundary conditions.

$$\theta^c_{1yy} + \theta^c_{1zz} = 0 \tag{99}$$

$$\theta^c_1(y,\ell) = 0 \tag{100}$$

$$\theta^c_1(y,0) = - y^{1/2} \tag{101}$$

$$\theta^c_1\,(y \to 0,\ z) = 0 \tag{102}$$

$\theta^c_1\,(y \to \infty,\ z)$ increases algebraically at most.

Equation (101) represents the interface temperature between aquifer region 3 and the clay cap. Equation (102) shows that the terms of 0 $(y_e^{\frac{1}{2}})$ disappear for $y \to 0$ as evident from (97).

The solution to the system of equations (99) to (102), obtained by using a Fourier sine integral transform with respect to y, is given as follows :

$$\theta^c_1\,(y,z) = -\frac{1}{2\ell}\left[\int_0^\infty \frac{\sin\frac{\Pi}{\ell}(\ell-z)\ \zeta^{1/2}\,d\zeta}{\cosh\frac{\Pi}{\ell}\left(|y-\zeta|\right) + \cos\frac{\Pi}{\ell}\,(\ell-z)}\right.$$

$$- \int_0^{\infty} \frac{\sin \frac{\Pi}{\ell}(\ell-z)\ \zeta^{1/2} d\zeta}{\cosh \frac{\Pi}{\ell}(y+\zeta) + \cos \frac{\Pi}{\ell}(\ell-z)} \Bigg] \tag{103}$$

A series solution, also obtained for the above system, can be written as

$$\theta_1^c(y,z) = \frac{1}{\ell} \sum_{n=1}^{\infty} \frac{1}{(-1)^n} \sin \frac{n\Pi}{\ell}(\ell-z) \int_0^{\infty} \zeta^{1/2} \left[\exp\left\{ - \frac{n\Pi}{\ell}(|y-\zeta|) \right\} - \exp\left\{ - \frac{n\Pi}{\ell}(y+\zeta) \right\} \right] d\zeta \tag{104}$$

An asymptotic solution for large values of y can be obtained directly from the system of equations (99) to (102). The same solution can also be developed by expanding (104) for $y \to \infty$. Substitution of such a solution in (98) results in the following expression for clay cap temperature:

$$\theta^c (y \to \infty, z) = 1 + \tau\left(1 - \frac{z}{\ell}\right) + y_e^{1/2} \sqrt{\frac{2}{\Pi}} \frac{\tau\lambda}{B\ell} \left[-y^{1/2}\left(1 - \frac{z}{\ell}\right) + \frac{1}{24y^{3/2}} \left(-3z^2 + \frac{z^3}{\ell} + 2\ell z\right) + 0\left(\frac{1}{y^{7/2}}\right) \right] + 0(y_e) \tag{105}$$

The temperatures in region 7 of the clay cap can be obtained by solving equation (49). Besides equation (50), another boundary condition is as follows.

$$\theta^c(\hat{y},0) = \theta_m(\hat{y}) \tag{106}$$

where $\theta_m(\hat{y})$ is the interface temperature between the clay cap region 7 and region 5 of the aquifer. $\theta_m(\hat{y})$ is calculated numerically at each step of $(\hat{y})$ for continuous heat flux and temperature at the interface. The 0(1) temperature solution in this region is:

$$\theta^c(\hat{y},z) = \theta_m(\hat{y}) + \frac{z}{\ell}\left[1-\theta_m(\hat{y})\right] \tag{107}$$

The temperatures in region 7 compatible with equation (105) can be obtained from (107) for small values of $\hat{y}$. The resulting expression is:

$$\theta^c(\hat{y} \to 0,\ z) = 1 + \tau\left(1 - \frac{z}{\ell}\right) - \sqrt{\frac{2d\hat{y}}{\Pi}}\ \frac{\tau\lambda}{B\ell}\left(1 - \frac{z}{\ell}\right) + 0(\hat{y}) \tag{108}$$

TEMPERATURE DISTRIBUTION IN THE AQUIFER

Once the velocity field in the aquifer is known the temperatures can be calculated from the energy equation. This must be done for five different regions shown in Figure 8. Since the effect of the surface cooling is limited to the boundary layer regions 1 and 3, the flow in regions 2 and 4 is isothermal. The solution structure in aquifer region 1 for $1 \leq \bar{y} \leq \infty$ appears to be more complex and will not be considered further because reasonable progress can be made without it. For all practical purposes, temperatures in aquifer region 1 can be assumed to be equal to those in fault region 1. The equation describing the thermal boundary layer in region 3 is:

$$\gamma^2\ v(z^*)\theta_y = y_e\ \theta_{yy} + \theta_{z^*z^*} \tag{109}$$

where

$$z^* = \frac{z}{y_e^{1/2}} \tag{110}$$

A similarity solution, compatible with equation (96) can be obtained for region 3. Elementary methods yield

$$\theta(y,z^*) = 1+\tau - \left(\frac{2yy_e}{\Pi}\right)^{1/2}\ \frac{\tau\lambda}{B\ell}\left[\sqrt{\frac{\Pi}{2}}\ B\eta\ \left\{1+\mathrm{erf}\ \left(\frac{B}{\sqrt{2}}\ \eta\right)\right\}\right.$$

$$+ e^{-\frac{B^2\eta^2}{2}}\Big] + O(y_e), \quad \eta = \frac{z^*}{y^{1/2}} \tag{111a,b}$$

It is possible to obtain an analytical solution of (42) in region 5, when $\hat{y} \ll 1$, and $z \ll 1$ such that $\frac{z}{\hat{y}^{1/2}} = O(1)$, which can be matched with (111a). We find the form

$$\theta(\hat{y},z) = 1 + \tau - \sqrt{\frac{2d\hat{y}}{\Pi}}\,\frac{\tau\lambda}{B\ell}\left[\frac{Bz}{\hat{y}^{1/2}}\sqrt{\frac{\Pi}{2d}}\left\{1 + \text{erf}\left(\frac{B}{\sqrt{2d}}\,\frac{z}{\hat{y}^{1/2}}\right)\right\}\right.$$
$$\left. + e^{-\frac{B^2z^2}{2d\hat{y}}}\right] + O(\hat{y}) \tag{112}$$

by using coordinate expansion methods.

The energy equation in (42), parabolic to the lowest order, must be solved subject to the boundary conditions in equations (45), (46) and (106) and the initial condition $\theta(\hat{y} \to o,z) = 1 + \tau$ for $|z| > 0$ obtained from matching with region 4. The last formal condition at the far end of the aquifer, (48) is used to determine a value of d. Numerical integration by standard finite difference methods is carried out for assumed values of d until the solution at the far edge is within 1% of the real condition and the heat flux and temperatures at the interface are continuous. This approximation provides an engineering type estimate of the boundary location. At that point, convection of energy associated with the $\theta_{\hat{y}}$ - term in (42) is very small compared to the conduction term. Of course, in the formal mathematical sense, the purely conductive profile can be found only for $\hat{y} \to \infty$. From the mathematical viewpoint, the reduction of the full-elliptic problem in the far-field aquifer to the parabolic system in (42) permits a simplified numerical computation procedure. The fact that

the reduction can be developed in a formal, rational manner for the large Rayleigh number approximation shows that the imposition of the far-field boundary condition at an *a priori* specified location is fundamentally unsound. That means, in physical terms, that the thermal anomaly associated with the upward fault zone flow has a natural horizontal relaxation length, associated basically with the distance required to transfer out of the surface, heat in excess of that arising from the natural geothermal gradient $\Delta T'/(\ell'+L')$. A quantitative indication of this matter involves the evaluation of d.

It is found that d is different for different sets of parameters as listed in Table 1. It can be observed from this table that an increase in M, R, τ or y_e increases d. Most notably, cases IV, I, V and VI in Table 1 show that d increases nearly linearly with growth in M, at least for $0.5 \leq M \leq 3$. It is clear that a longer aquifer is needed for the transition to the conduction temperature profile when any parameter except λ in Table 1 is increased. In physical terms this result implies that the hot isothermal portions of the aquifer, maintained by horizontal convection effects, will be more extensive in systems of relatively larger mass flow, permeability, temperature difference, and fault size. An increase in λ is associated with a decrease in d. Faster convergence to the far-field boundary condition occurs because of increased cap heat transfer. A reduction in cap heat transfer caused by an increase in cap thickness implies that a longer aquifer (or increase in d) is required to stabilize the temperatures, as confirmed by Table 1.

Table 1. Values of d for Different Sets of Parameters

Case No.	d	ℓ	λ	M	R	τ	y_e
I	0.24	0.24	0.7	1	500	1	0.025
II	0.28	0.50	0.7	1	500	1	0.025
III	0.22	0.24	1.0	1	500	1	0.025
IV	0.14	0.24	0.7	0.5	500	1	0.025
V	0.49	0.24	0.7	2	500	1	0.025
VI	0.74	0.24	0.7	3	500	1	0.025
VII	0.18	0.24	0.7	1	338	1	0.025
VIII	0.50	0.24	0.7	1	1000	1	0.025
IX	0.24	0.24	0.7	1	500	0.6	0.025
X	1.04	0.24	0.7	1	500	1	0.05
XI	0.32	0.24	0.7	1	338	0.6	0.034

RESULTS AND THEIR COMPARISON WITH THE FIELD DATA

The distribution with depth of the nondimensional aquifer velocity and of temperature in the aquifer and clay cap are shown in Figures 9 to 12. Parameters used in these plots are those calculated previously for the East Mesa anomaly. In Figure 9 we observe a significant distribution with depth of the velocity in the aquifer. This configuration is determined by the vertical distribution of the horizontal pressure gradient in the aquifer. The gradient near the top of the aquifer is relatively large because of the stagnation point effect near the top of the fault zone. It should be noted that this result has been obtained for an aquifer at constant horizontal permeability. One may speculate that a reduction in deep permeability will reduce the high velocity in the lower portion of the system. The dimensional value of the mass flow rate per unit area can be obtained by multiplying the nondimensional velocity of Figure 9 by $y_e\, q'_o \rho'_o$.

Figure 10 shows the variation of the aquifer and clay cap temperatures with depth at several horizontal locations for the parameter set shown. The value $\hat{y} = 1$ represents the far end of the aquifer, which is located at $(d/y_e)L' = (9.41)(3.35\text{km}) = 31.5$ km. Even at $\hat{y} = 0.6$ (18.9 km) the temperature profile is nearly at the conduction value. The temperature decreases with distance from the fault at a given depth in the aquifer which is a result of heat loss through the clay cap. It may be noted that at 10% out in the aquifer, the bottom 60% of the reservoir is still within about 94% of the high temperature value. A qualitative comparison of Figures 5 and 10 implies that the hot wells, 48-7, 6-1, 6-2, 8-1, and 44-7, are located in or near the fractured fault zone. Relatively flat temperature profiles in Mesa wells 8-1, 44-7, and 48-7 below about 0.95 km can be interpreted as resulting from the near-fault zone flow. It is important to recognize that

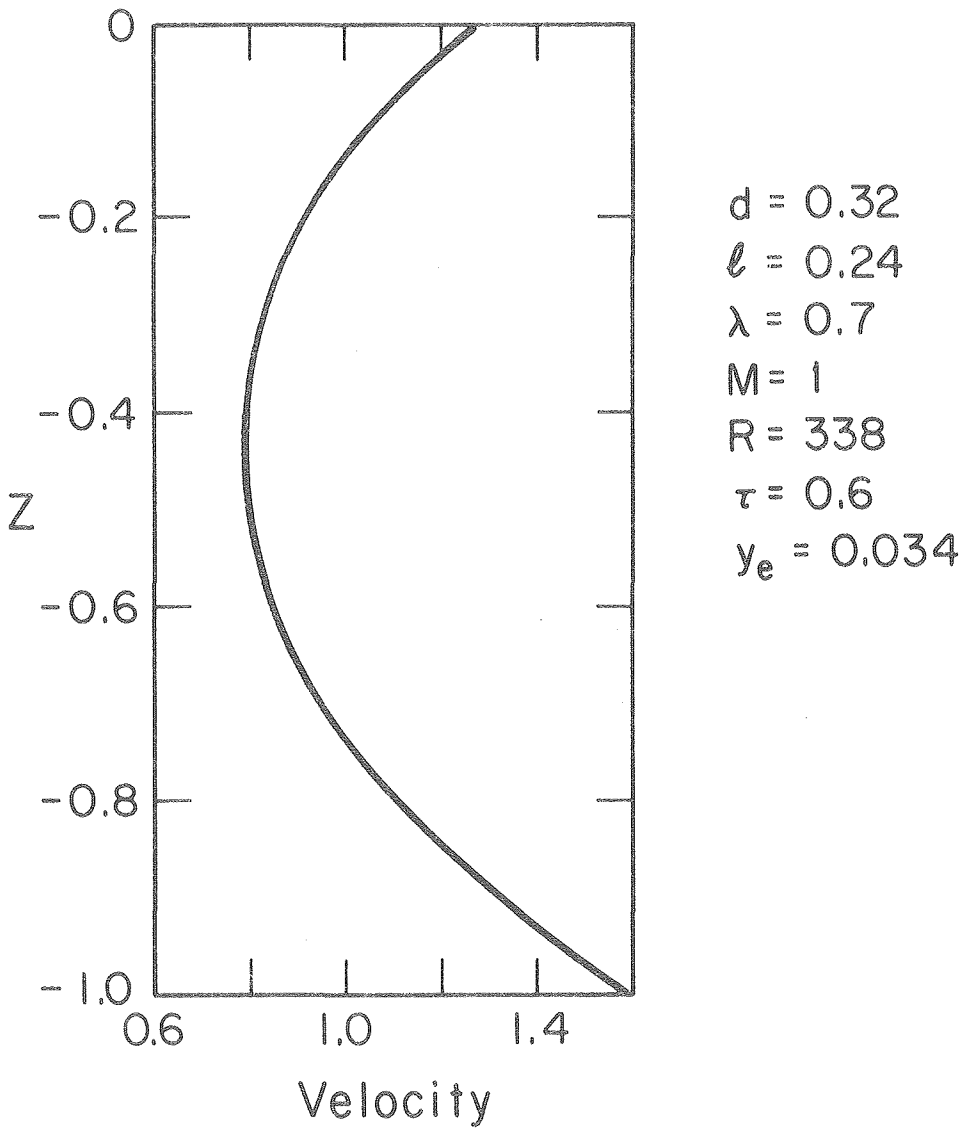

Figure 9. Horizontal velocities in the aquifer.

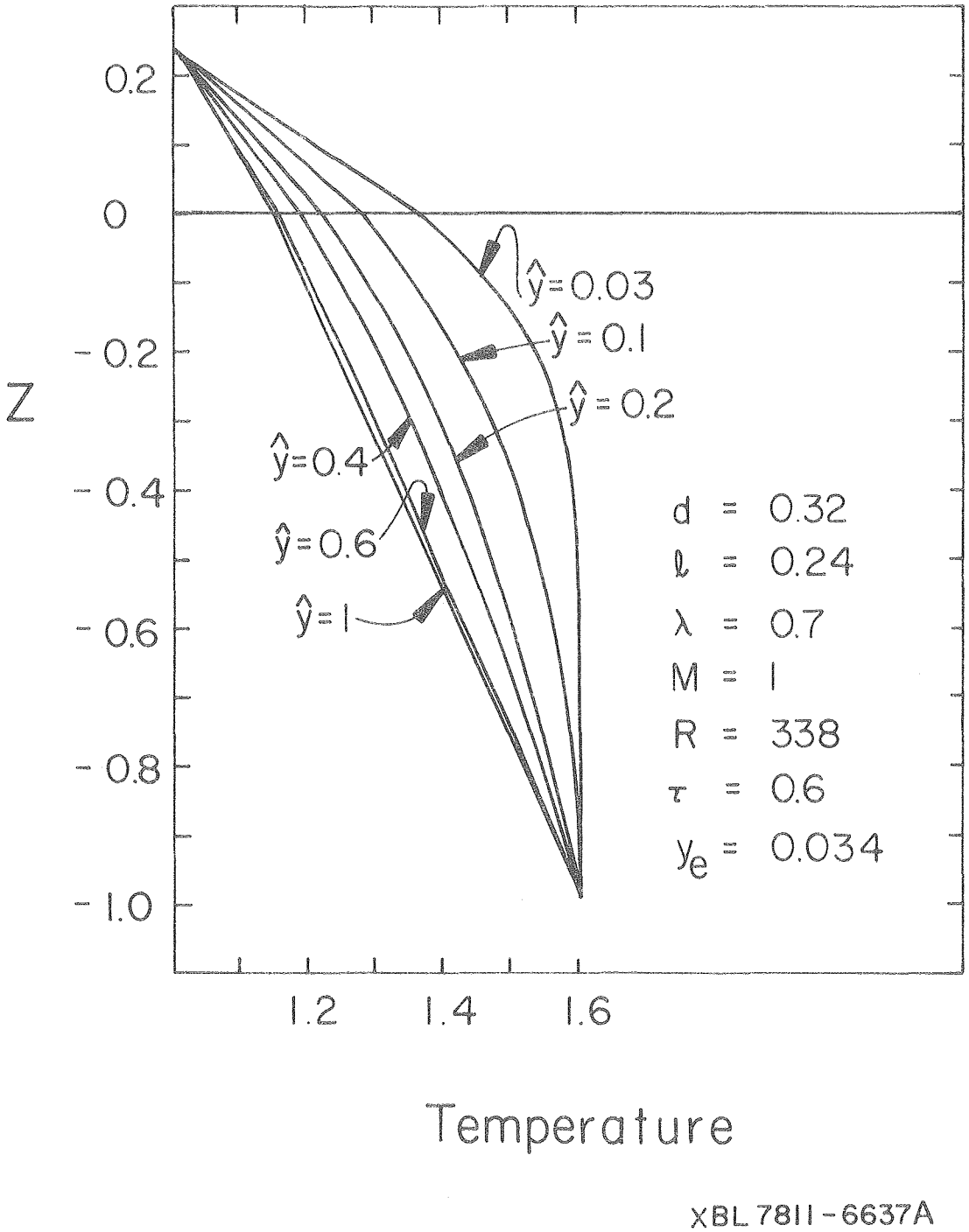

Figure 10. Temperatures in the aquifer and clay cap for different values of $\hat{y}$.

these flat temperature profiles can occur in regions of purely horizontal flow as long as the bore is reasonably close to the hypothesized fault zone. One may observe from Figure 10 that even at $\hat{y} = 0.1$ (3.15km) the lower part of the temperature profile is relatively flat. Temperature profiles for $\hat{y} > 0.2$ (Figure 10) are similar to those of remaining wells in Figure 5, indicating that these wells are further away from the fracture zone. In particular well 18-28 is the farthest from any known fault zone. The nondimensional mass flux value M=1 corresponds to an input at the bottom of the fault of 11.44 kg/sec for each kilometer of horizontal extent. This value is quite similar to the estimate used by Riney et al., [1979a] in a recent study of the northwest lobe of the Mesa system. The isotherms corresponding to the temperatures of Figure 10 are shown in Figure 11. It is apparent in this figure that the horizontal temperature gradient decreases as the liquid moves away from the fault and becomes negligibly small near the far end. The near-fault isotherm values are calculated from the boundary layer solutions of regions 1, 3, and 6.

The temperature gradients at the cap surface are shown in Figure 12. The discontinuity in the curve arises because the solutions in aquifer regions 3 and 5 and clay cap regions 6 and 7 have been calculated to different orders of accuracy in the asymptotic analysis. It is found that an increase in M, R, τ, and y_e enhances the temperature gradients at the surface while an increase in ℓ and λ decreases the temperature gradients there, as expected. In Figure 12 we see that the fault zone convection process enhances the surface heat flux by a factor of about 4 above the background conductive value. A similar ratio can also be obtained from Figure 2 where the near-fault heat transfer is about 8 heat flow units (HFU) compared to the background value of 1.5 to 2.0 HFU.

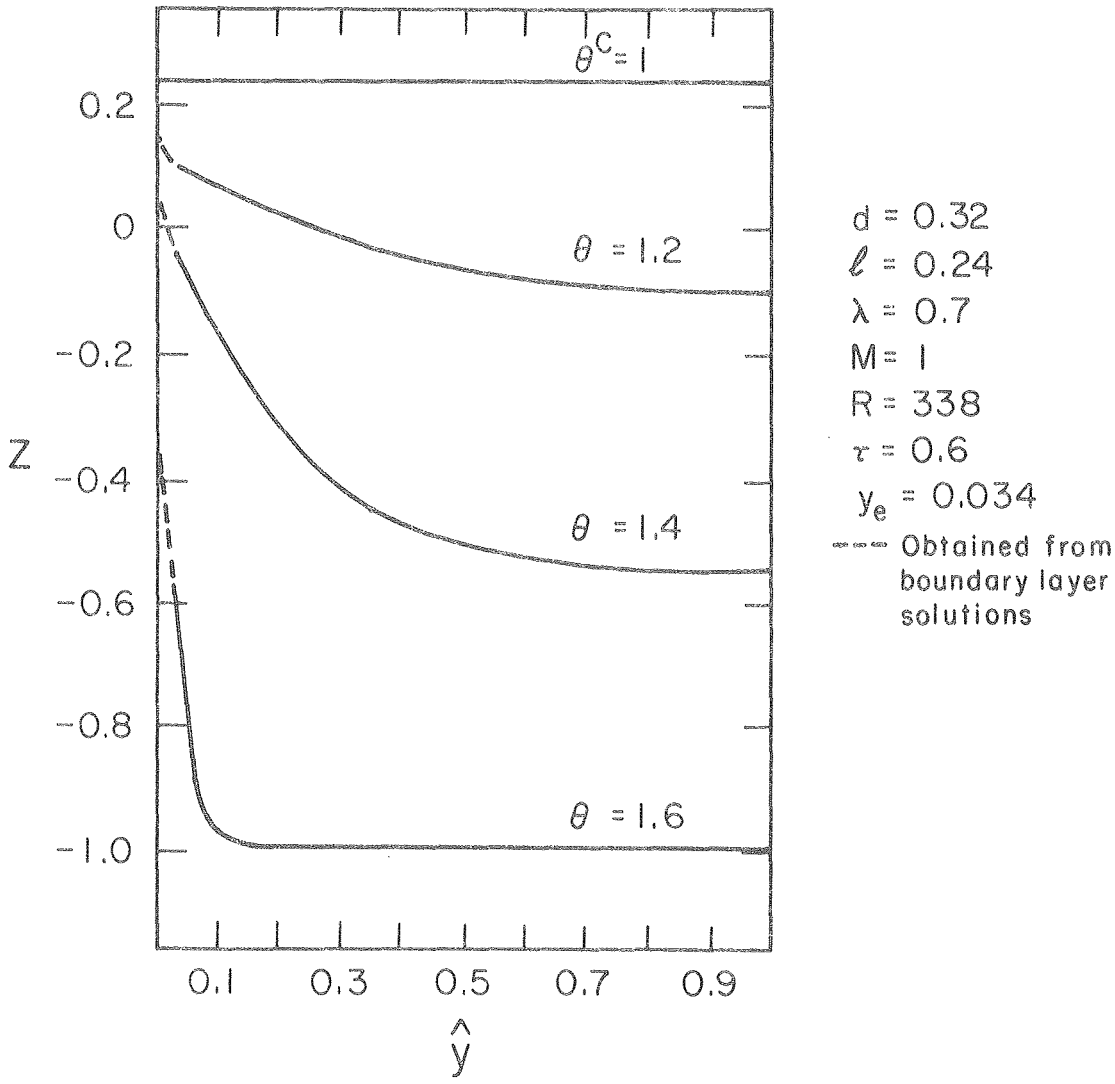

Figure 11. Isotherms in the aquifer and the clay cap.

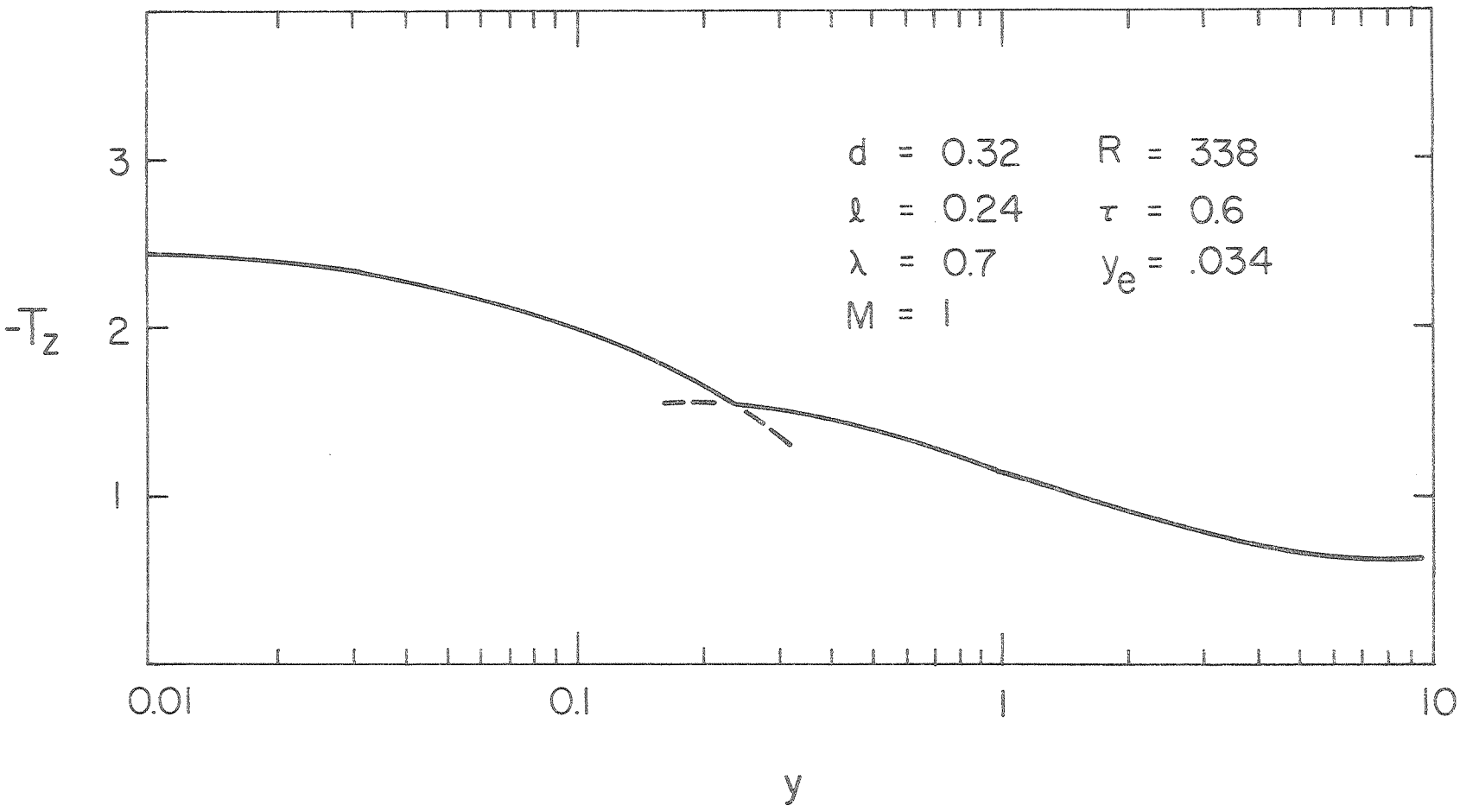

XBL 7811-6633A

Figure 12. Surface temperature gradients along the length of the aquifer.

Heat flux contours measured in the proximity of the East Mesa wells are shown in Figure 13. A plot of heat flux versus distance along three lines ①, ② and ③ of Figure 13 is given in Figure 14. The surface heat flux predicted from the theory is also shown in Figure 14 along with the related parameters. This comparison shows that heat flux in field observations is somewhat larger than predicted. The discrepancy can arise for a variety of reasons. In this analysis we have considered the reservoir to be a zone of constant horizontal permeability while the field data shows the existence of two distinct zones of permeability (Figure 6). For a given mass input M we would expect more hot liquid to pass through the upper, more permeable section, thus increasing the surface heat flux. Liquid transport properties are assumed to be constant in our model. However, to some extent the decrease of viscosity with depth (temperature) compensates for the actual decrease in permeability deep in the system. The actual mass flow rate in the field may be different than 9.89×10^5 kg/day-km used in Figure 14. It is clear on physical grounds that a larger mass flux would increase the surface heat flux. This is verified theoretically by the solution in (98). Most significantly, the planar geometrical configuration used in the model, representing flow up to a vertical narrow fault and into adjacent aquifers, is not an accurate representation of the localized northwest lobe from which the data in Figure 14 is obtained. In all probability, an axisymmetric model, like that used by Riney et al. [1979b]would be more compatible with the local system. Also, it appears that the Rex and Babcock faults (Figures 2 and 13), as well as the Mesa fault contribute to the anomaly. This seems reasonable since the hottest wells, 44-7 and 48-7, lie near the intersection of the Rex and Babcock faults (Figures 2 and 13). In retrospect it seems that the

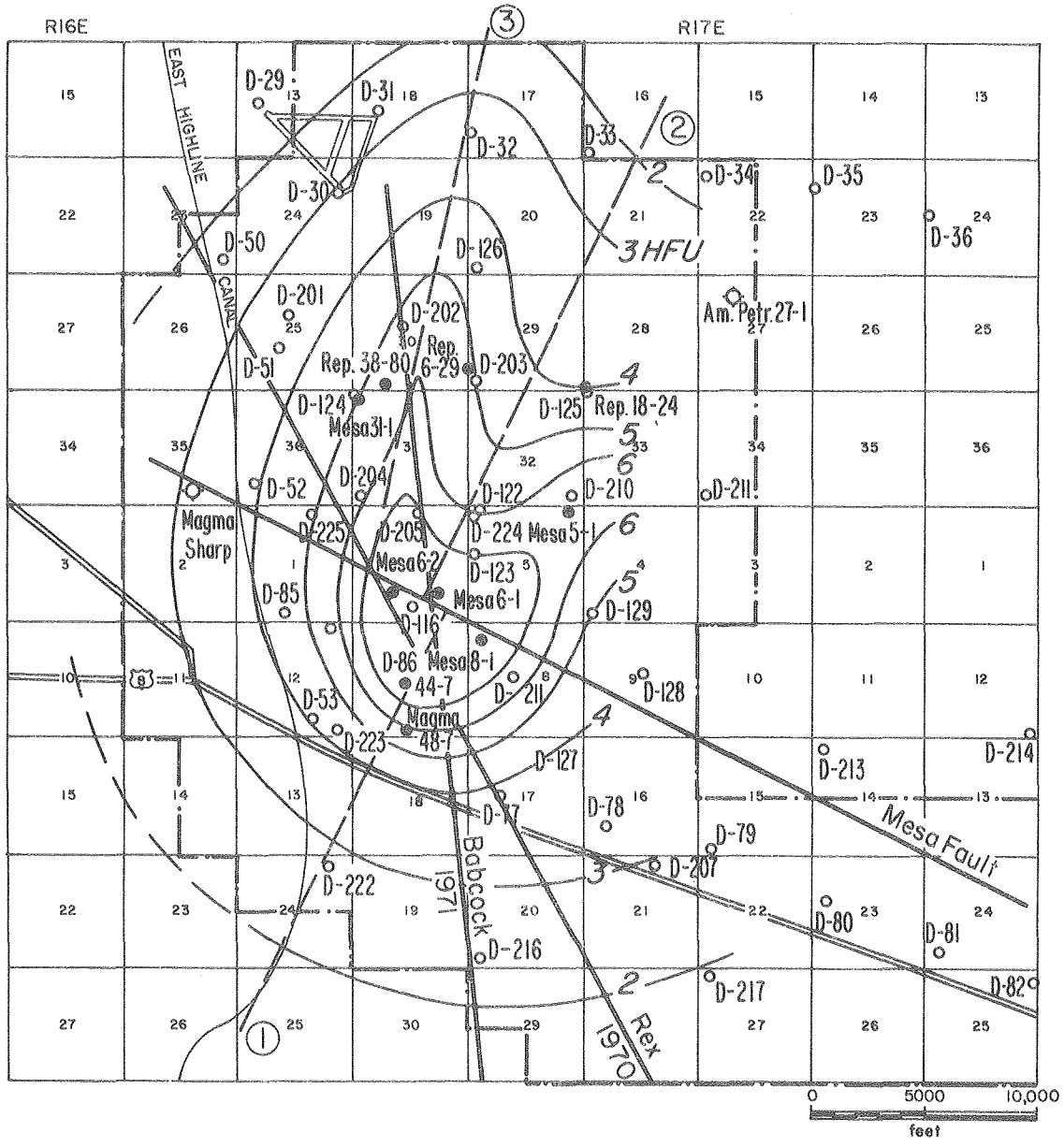

Figure 13. Heat flow contours measured in the proximity of East Mesa wells. (Adapted from Pearson, [1976].)

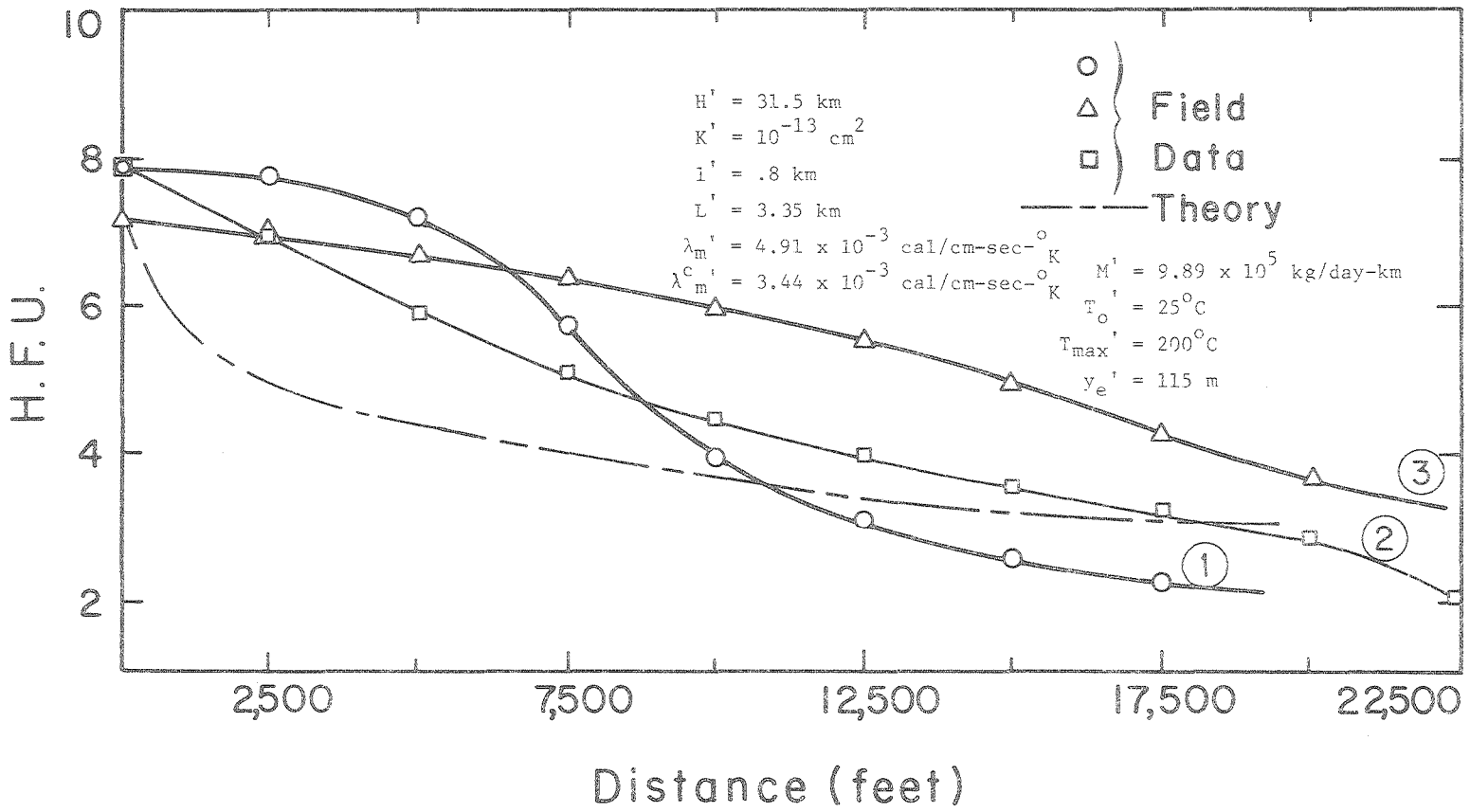

XBL 792-7366

Figure 14. A comparison of the calculated surface heat flux to that measured in the field along lines ①, ② and ③ of Figure 13.

the mass input value were not chosen in a way that would specifically encourage the predicted results to agree with the field measurements. In particular, no special distributions of temperature or heat flux on the upper or lower boundaries were considered in order to improve the agreement. Nor was an attempt made in this model to manipulate the permeability distributions in the aquifer. That we obtain results reasonably similar to the observations without iterating these constraints suggests that the conceptual model is physically plausible.

In a related study by Riney et al. [1979a], described in more detail in Riney et al. [1979b], a conceptual model similar to that used here is developed for the Mesa system. The mathematical model is based on a cylindrical, axisymmetric geometry with fracture zone-type upflow localized near the center. The effects of variable fluid properties and spatially-dependent material properties (permeability and porosity), are included. At the aquifer bottom, the temperature decreases slowly with increasing radial distance from the origin. Other boundary conditions are like those employed in the present work, although the location of the far-field boundary at a radial distance of 10 km is selected a priori. A finite difference technique based on line-successive overrelaxation is used to develop solutions. The computations are carried out for a mass input, obtained from an overall energy balance, of 16.9 kg/sec. at 469.26°K. A variable-size grid, basically 5 cells high and 13 cells long, is used in the computation. Results are presented for a variety of spatial distributions of the vertical and horizontal permeability. It was found that intrusion of deep cold water from the far-field boundary could occur if there was adequate vertical permeability in the system. In this case, there was inflow in the

deep section and outflow in the shallow section such that the net mass flux at the far boundary was just equal to the input value. This partial convective circulation cell results from the propensity of a system with a hot bottom temperature, highest near the axis, cold top, and open side boundary to develop a natural convection mode. Cheng and Lau [1974] have considered a related problem. The associated prediction of an inverted temperature profile at depth is not compatible with known field data. It was concluded that only a very minimal vertical permeability, 0.3-0.5 milli darcy, relative to a maximum horizontal value of 90 md was needed to model the Mesa system. This conforms with the known geological structure in the area. The flow pattern in this case involves outflow through the aquifer depth. Vertical permeability reduction leads to the suppression of the natural convection mode. An excellent reproduction of the surface heat flux pattern was obtained by carefully tailoring the spatial distribution of vertical and horizontal permeability. In general the results obtained are qualitatively similar to those found in the present work. It is reasonable to conclude that fault zone controlled charging of a geothermal reservoir is at least plausible if not a fact.

SUMMARY

A conceptual model of fault-zone-controlled charging of a geothermal reservoir, based on data from the East Mesa system, has been developed. The mathematical model is based on flow in a liquid-saturated porous medium. A two-dimensional, vertical, planar geometry is considered. The problem formulation is based on perturbation methods and asymptotic procedures valid in the limit of large Rayleigh number and small values of

the nondimensionalized fault width. Both analytical and numerical methods are employed to develop solutions for the velocities, pressures, and temperatures in the field. There is better than qualitative agreement between predictions of variation of temperature-depth profiles with distance from the fault, and surface heat flux patterns with the associated field data. It is shown that flat temperature profiles at depth can be associated with purely horizontal water motion (Darcy flow rate of about 0.01 cm/day near to hypothesized faults) rather than only with the more rigorous upflow itself. Although the model used here lacks the various elements of reality discussed earlier, the comparison of prediction and field data is quite reasonable. We are led to believe that the model is a plausible generic type that may be useful in considering other systems as well. In particular, we believe that improved interpretation of field data may be possible by utilizing some of the physical ideas presented here.

Acknowledgment: This work was supported by the Assistant Secretary for Resource Application, Office of the Division of Geothermal Energy of the U. S. Department of Energy under Contract W-7405-ENG-48 administered by Lawrence Berkeley Laboratory as part of the Laboratory's Geothermal Reservoir Engineering Management Program ("GREMP"). Manuscript development was supported in part (for D. R. Kassoy) by the U. S. Geological Survey Extramural Geothermal Program through Grant #14-08-001-0628.

REFERENCES

Bailey, T. P., A hydrogeological and subsurface study of Imperial Valley geothermal anomalies, Imperial Valley, California: Report CUMER77-4 p. 101, Geological Sciences, University of Colorado, Boulder, 1977.

Biehler, S., Gravity studies in the Imperial Valley in cooperative geological-geophysical-geochemical investigations of geothermal resources in the Imperial Valley of California, Final Report, Contract No. 14-06-300-2194 United States Bureau of Reclamation, pp. 29-42, University of California, Riverside, 1971.

Black, H. T., A subsurface study of the Mesa Geothermal Anomaly, Imperial Valley, California: CUMER 75-5, p. 58, Geological Sciences, University of Colorado, Boulder, 1975.

Cheng, P. and K. H. Lau, Steady State free convection in an unconfined geothermal reservoir, J. Geophysical Res., 79,(29), 4425-4431, 1974.

Combs, J., Thermal studies in cooperative investigations of geothermal resources in the Imperial Valley Area and their potential value for desalting of water and other purposes, UCR/IGPP 72-33, pp. B-1 to B-23, University of California, Riverside, 1972.

Combs, J., Seismic refraction and basement temperature investigation of the East Mesa Known Geothermal Resources Area, Southern California: Transactions, vol. 1, pp. 45-47, Geothermal Resources Council, 1977.

Combs, J., and D. Hadley, Microearthquake investigation of the Mesa Geothermal Anomaly, Imperial Valley, California, Geophysics, 42, (1) 17-33, 1977.

Corwin, R. F., H. F. Morrison, S. Diaz, C., and J. Rodriguez B., Self potential studies at the Cerro Prieto Geothermal Field, in Proceedings of the First Symposium on the Cerro Prieto Geothermal Field, Baja California, Mexico, held at San Diego California, LBL-7098, Lawrence

Berkeley Laboratory, Berkeley, California, pp. 204-210, 1978.

Davis, D. G., and S. K. Sanyal, Case history report on East Mesa and Cerro Prieto Geothermal Fields, LA-7889-MS (informal report), Los Alamos Scientific Laboratory, Los Alamos, New Mexico, 1979.

Elders, W. A., J. R. Hoagland, E. R. Olson, S. D. McDowell, And P. Collier, A comprehensive study of samples from geothermal reservoirs, UCR/IGPP-78/26, University of California, Riverside, pp. 264, December 1978.

Goyal, K. P., Heat and mass transfer in a saturated porous medium with applications to geothermal reservoirs, Ph. D. thesis, Mechanical Engineering Department, University of Colorado, Boulder, p. 294, 1978.

Goyal, K. P., and D. R. Kassoy, Fault zone controlled charging of a liquid dominated geothermal reservoir: J. Geophysical Res. 85(B4) pp. 1867-1875, 1980.

Howard, J., J. A. Apps, S. Benson, N. E. Goldstein, A. N. Graf, J. Haney, D. Jackson, S. Juprasert, E. Majer, D. McEdwards, T. V. McEvilly, T. N. Narasimhan, B. Schechter, R. Schroeder, R. Taylor, P. Van de Kamp and T. Wolery, Geothermal resource and reservoir investigations of U.S. Bureau of Reclamation leaseholds at East Mesa, Imperial Valley, California, LBL-7094, Lawrence Berkeley Laboratory, Berkeley, California, p. 305, October 1978.

Martinez Baez, L. F., Thermal conductivity of core samples from the Cerro Prieto Geothermal Field: Experimental results and an improved prediction method, in Proceedings of the First Symposium on Cerro Prieto Geothermal Field, Baja, California, Mexico, held at San Diego, California, LBL-7098, Lawrence Berkeley Laboratory, Berkeley, California, pp. 342-351, 1978.

Meidav, T., and R. B. Furgerson, Electrical resistivity for geothermal exporation in the Imperial Valley, in Cooperative geological-geophysical-geochemical investigations of geothermal resources in the Imperial Valley of California, Final report Contract no. 14-06-300 2194, U. S. Bureau of Reclamation, pp. 43-83, University of California, Riverside, 1971.

Morrison, H. F., R. F. Corwin, R. Harding, and G. Demonlly, Interpretation of self potential data from geothermal areas, semi-annual technical progress report, USGS Contract #14-08-0001-16546, University of California, Berkeley, 1979.

Pearson, R. O., Planning design of East Mesa geothermal test facilities (Phase 1B), vol. 1 of TRW Inc. Final Report, Energy Research and Development Administration (Department of Energy) contract no. E(04-3)-1140, 1976.

Riney, T. D., J. W. Pritchett, L. F. Rice, and S. K. Garg, A preliminary model of the East Mesa hydrothermal system, in Proceedings Fifth Workshop Geothermal Reservoir Engineering, SGP-TR-40, Stanford University, Stanford, California, pp. 211-214, 1979a.

Riney, T. D., J. W. Pritchett, L. F. Rice, and S. K. Garg, Integrated model of the shallow and deep hydrothermal systems in the East Mesa Area, Imperial Valley, California, Semi-Annual Tech. Report #1, SSS-R-79-3995, Systems, Science and Software Inc., Box 1620, La Jolla, California, 92038, 1979b.

Smith, J. L., Geology and commercial development of the East Mesa Geothermal Field, Imperial Valley, California, in Geology and Geothermics of the Salton Trough, Geological Society of America, 92nd Annual Meeting, San Diego, W. A. Elders, editor, pp. 86-94, 1979.

Somerton, W. H., and A. H. El-Shaarani, High temperature behavior of rocks associated with geothermal type reservoirs, Paper No. SPE 4897, presented at the 44th Annual California Regional Meeting of the Society of Petroleum Engineers of AIME San Francisco, California, April 4-5, 1974.

U.S. Bureau of Reclamation, Geothermal resource investigations, Imperial Valley, California: Developmental Concepts, p. 57, Washington D.C., U.S. Department of the Interior, Bureau of Reclamation, January 1972.

U.S. Bureau of Reclamation, Geothermal resource investigations, Imperial Valley, California: Special report, Test Well Mesa 6-1, p. 44, Washington D.C. U.S. Department of the Interior, Bureau of Reclamation, February 1973.

U.S. Bureau of Reclamation, Geothermal resource investigations, Imperial Valley, California: Status report, p. 63, Washington D.C., U.S. Department of the Interior, Bureau of Reclamation, November 1974.

U.S. Bureau of Reclamation, Geothermal resource investigations, Imperial Valley California: Status report, p. 99, Washington D.C., U.S. Department of the Interior, Bureau of Reclamation, 1977.